Nano Research
2023, 16(4): 4365–4380

ISSN 1998-0124 CN 11-5974/O4
https://doi.org/10.1007/s12274-022-5082-z

Mini Review

The cathode catalysts of hydrogen fuel cell: From laboratory toward practical application

Shuang Cao[1,§], Tong Sun[1,§], Jin-Rong Li[1], Qin-Zhu Li[1], Chun-Chao Hou[2] (✉), and Qi Sun[1] (✉)

[1] College of Chemistry and Chemical Engineering, Institute for Sustainable Energy and Resources, Qingdao University, Qingdao 266071, China
[2] School of Materials Science and Engineering, Ocean University of China, Qingdao 266100, China
[§] Shuang Cao and Tong Sun contributed equally to this work.

Received: 2 August 2022 / **Revised:** 6 September 2022 / **Accepted:** 20 September 2022

ABSTRACT

Proton exchange membrane fuel cells (PEMFCs) have received a sustained world-wide attention owing to their promising applications based on clean energy. However, their widespread applications are still restricted by the sluggish oxygen reduction reaction (ORR) process. Over the past decades, significant efforts have been devoted to developing efficient ORR catalysts, which have been summarized in numerous previous reviews. Unfortunately, most of them mainly focused on ORR activity on the rotating disk electrode (RDE) level, which cannot truly represent the performance in real applications. Developing and showcasing efficient catalysts evaluated at the membrane electrode assembly (MEA) level is of vital importance. In this review, we first briefly showcased the recent development of ORR catalysts and then put more emphasis on the discussion of designing efficient catalysts at MEA and full-cell level, aiming to help stimulate more attention on their practical applications.

KEYWORDS

oxygen reduction reaction, hydrogen energy, membrane electrode assembly, proton exchange membrane fuel cells

1 Introduction

With the growth of global population and economic expansion, the energy and environment are under severe threat due to the excessive consumption of fossil energy. Therefore, it is urgently demanded to develop environment-friendly and sustainable energy technologies. Green hydrogen, generated through solar and wind energies or from biomass waste conversion, is one of the most promising energy carriers to build an absolutely zero-emission and sustainable economy [1–3]. Hydrogen fuel cells, which can convert the chemical energy of hydrogen into electricity without the limitation of the Carnot cycle, show great potential as power sources. In particular, the proton exchange membrane fuel cells (PEMFCs) have attracted enormous interest owing to the high density, sufficient efficiency, and zero environmental impact. The values of the vehicles are greatly influenced by the performance of PEMFCs. Up to now, the hydrogen fuel cell electric vehicles (HFCEVs) have achieved commercialization. However, to realize broader application, several key issues are still existing to hinder further technological breakthrough. Particularly, the cathodic oxygen reduction reaction (ORR), which is in the heart of the electrochemical conversion processes, determines the overall performance of the cells and remains the roadblock to the wide application of this promising technology.

Since the Pt was introduced as the fuel cell catalyst by William R. Grove in 1840s, it remains the most widely used and best-efficient catalyst in PEMFCs [4]. However, the large amount of Pt usage puts substantial limitation on the broad application of PEMFC techniques, because it takes up about 40%–50% of the overall fuel-cell stack cost [5]. Therefore, over the past decades, enormous effort has been made to develop low-cost ORR electrocatalysts and achieved efficient catalytic activities. Nevertheless, it should be noticed that most of reported works are devoted to the performance of catalysts on the rotating disk electrode (RDE) level, which cannot be directly translated to the membrane electrode assembly (MEA) and fuel-cell performance, since there are several differences between RDE and MEA measurements, such as mass transfer (O_2 diffusion) resistance, catalyst layer, concentration of O_2, and operating temperature. Consequently, the insufficient data on the real MEA and fuel-cell performance becomes a serious impediment for its development. Although most of researchers have realized it, the corresponding improvement remained stagnant and most of the investigations are still on the laboratory level. Therefore, it is of great significance to make insightful investigations on MEA and fuel-cell test.

In this review, we first summarize the fundamental points and development of ORR catalysts and then discuss their advantages and insufficiencies in practical applications. Then we put more emphasis on the discussion of ORR catalysts on MEA or fuel cell level and discuss the important issues of developing catalyst from RDE to MEA and fuel-cell level. We hope it can help stimulate more attention in this field and promote significant development of more desirable catalysts for the widespread practical applications of PEMFCs in the near future.

1.1 Introduction of a hydrogen fuel cell

The complex hydrogen fuel cell system mainly consists of fuel cell stack, gas supply system, and control system, among which the

Address correspondence to Chun-Chao Hou, houchunchao@hotmail.com; Qi Sun, qisun_l@hotmail.com

fuel cell stack is the core component and it accounts for ~ 60% of the total cost of fuel cell (Fig. 1(a)). For a fuel cell stack system, it mainly includes bipolar plates, MEA, and packaging. The MEA is the core component, which consists of gas catalyst layer, proton (ion) exchange membrane, and gas diffusion layers (Fig. 1(b)) [6]. In practical application, the cell mainly operated in the low-current-density regions, and the catalytic ORR activity at cathode strongly influences the energy conversion efficiency of fuel cell [6].

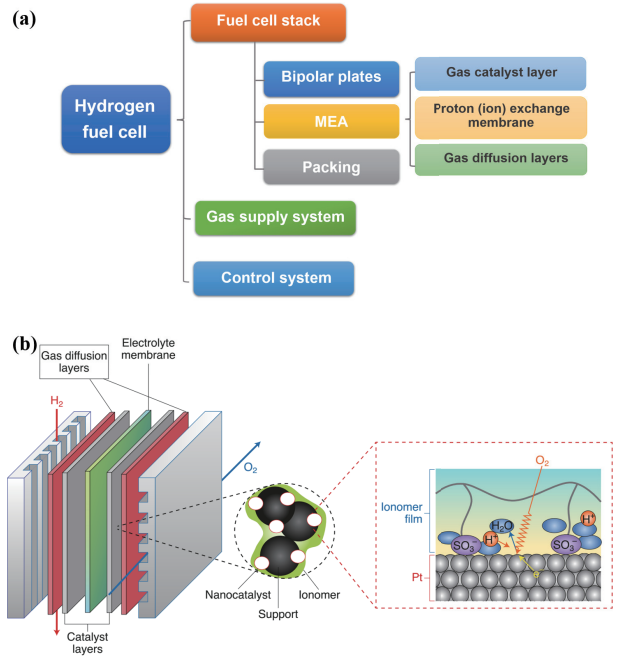

Figure 1 (a) Schematic and (b) configuration of the PEMFC (the middle inset in (b) represents the microstructure of a cathode catalyst layer). Reproduced with permission from Ref. [6], © Kodama, K. et al. 2021.

Since the efficiency of cathodic ORR reaction dominates the overall performance of the fuel cell, therefore, developing robust ORR electrocatalysts with low price is decisive to extend application of this clean and sustainable energy technology. Up to now, the most widely used catalysts in practical acidic PEMFCs are still novel metals, such as platinum group metals (PGMs), whereas, its cost is responsible for up to ~ 23% of the fuel cell's expenses and is the main source of the fuel cell cost. Decreasing the amount of Pt utilization is the core to the broader usage of PEMFCs. However, most low-cost catalysts are usually unstable in acidic conditions, especially used in acidic fuel cell devices. Consequently, it is a great challenge to develop robust catalysts with good durability without sacrificing the performance and cost.

1.2 The catalytic kinetics and mechanism of ORR

The mechanism of ORR involves two pathways named four-electron pathway (pathways (1) and (2) in Fig. 2(a)) and two-electron pathway (pathway (3) in Fig. 2(a)), which produce H_2O and H_2O_2, respectively [7].

Effective four-electron pathway

$$O_2 + 4H^+ + 4e^- \rightarrow 2H_2O$$

Ineffective two-electron pathway

$$O_2 + 2H^+ + 2e^- \rightarrow H_2O_2$$

$$2H_2O_2 + 2H^+ + 2e^- \rightarrow 2H_2O$$

Both of the oxygen reduction pathways are possible for different kinds of catalysts. In practical application, the desired ORR pathway is the four-electron pathway. However, the two-electron

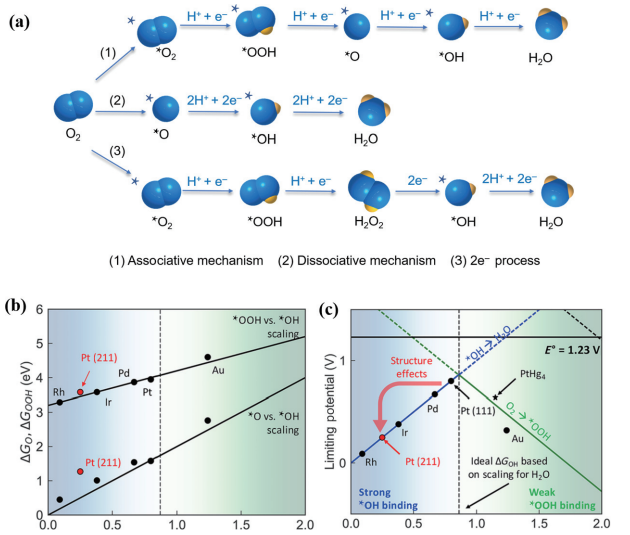

Figure 2 (a) Illustration of the different reaction pathways of the ORR. The signal of * means the adsorbed state. (b) The chemisorption energy relationships of *OOH vs. *O and *O vs. *OH for the (111) surface of the typical metals (Rh, Pt, Ir, Pd, Pt, and Au). (c) The relationship between the strongly bound *OH region (solid blue line) and weakly bound *OOH region (solid green line) for the four-electron process. Reproduced with permission from Ref. [12], © American Chemical Society 2018.

pathway is unavoidable no matter for PGM or low-cost ORR catalysts. It is speculated that many factors, such as crystal faces, defects, and the amounts of active sites, relate to this ORR pathway [8–10]. Typically, for an indirect two-electron reduction pathway, O_2 molecules adsorbed on the surface of catalysts first can be reduced to H_2O_2, which then transforms to H_2O. By contrast, for the direct four-electron ORR, the O_2 can be reduced through either a dissociative or an associative route, depending on whether the O–O bond dissociates before or after the protonation (Fig. 2(a)) [11]. When the O_2 binds on the surface strongly or the surface oxygen coverage is low, the dissociation pathway is favored, otherwise, the association pathway is preferred [12]. During the associative reaction, three different intermediates (*O, *OH, and *OOH) are involved, whereas, only *O and *OH are involved in the dissociative pathway. Because these multiple oxygen intermediates bind to the surface through O atom similarly and their binding energies can be revealed by a "scaling relationship". The slopes are close to 1 and 2 for the lines of *OOH vs. *OH and *O vs. *OH, respectively (Fig. 2(b)), which indicates the *OOH and *OH have a similar metal–oxygen single bond and *O has a double bond to the surface [12, 13]. In general, only one adsorbate is introduced to explain the adsorption energy of all intermediates and products [12]. For ORR, the *O binding free energy is initially to describe the catalytic activity. Afterwards, because of the better scaling between *OOH and *OH, the *OH binding free energy has become a more convenient indicator to illustrate the variations of electronic structure between different catalysts. However, it should be noticed that the adsorption energies of *OH and *O are essentially related to the states of metal d-band center (ε_d) associated with the bonding [14]. Neither too high nor too low binding energy of these intermediates are suitable for the high activities of ORR, which follows the "Sabatier principle" [15]. As shown in Fig. 2(c), *OH → H_2O is the potential limiting process (solid blue line) when the metal binds *OH strongly and O_2 → *OOH is potential limiting (solid green line) for the weakly bonding metals [12].

2 ORR catalysts

In this review, we mainly discuss the ORR catalysts from the following four aspects: PGM-based catalysts, non-PGM catalysts, carbon-based (C-based) catalysts, and single-atom catalyst (SACs).

2.1 PGM-based catalysts

To date, Pt is still the benchmark and demonstrates the best performance among the PEMFCs catalysts. To further improve the intrinsic activity and active sites of the Pt catalysts, the strategies of reducing the particle size, alloying, and optimizing its shape are widely accepted. For example, in practical application, to control the particle size and reduce aggregation, the Pt nanoparticles (NPs) are usually loaded on carbon blacks with high surface area. More importantly, the comprehensive understanding of the ORR process on the surface of the catalysts plays a significant role in designing highly active and stable catalysts. Over the past decades, enormous experimental and theoretical researches have focused on it. The theories for the design of highly active Pt-based catalysts are mainly based on d-band theory.

The d-band theory describes the relationship between the d-states of the transition metals and the surface adsorbates. Since all transition metals have similar broad sp-bands, it can be speculated that they have little influence on the adsorption behavior between different metals. Therefore, the energy level of d-bands plays a main role in regulating the adsorption behaviors. It is widely accepted that the ε_d is relative to the Femi-level, which represents the average energy of the d-band. In general, the adsorption strength of oxygen species on the catalyst surface can be regulated by the surface electronic structure (d-band) of the metals and then the ORR activity can be modified. For the same metal, the ε_d mainly depends on the d-band bandwidth (W_d), which is in proportion to the interatomic matrix element (V_i). Therefore, the relationship between ε_d, coordination number (CN), the characteristic length (r_d), and the distance between the atoms (d_{ij}) can be illustrated by the following equation (the i and j represent the atomic arrangement of the surface atom and its neighboring atoms, respectively) [4]

$$|\varepsilon_d| \propto W_d^{0.5} \propto V_i = \sum_{j=1}^{CN} \frac{(r_{d,i} r_{d,j})^{1.5}}{d_{ij}^5}$$

Based on this theory, the improvement of ORR performance for Pt-based catalysts mainly focuses on the ε_d modulation through facet effect, ligand effect, and strain effect [4].

2.1.1 *Facet effect*

In 1979, Ross et al. first studied the structure sensitivity toward ORR and its relationship with the CN of surface atoms for three low index Pt planes [16]. However, because the Pt surface became rough at high cycling potential (0–1.5 V vs. reversible hydrogen electrode (RHE)), the results showed the same activity for different planes. Then, the experiment was improved by Yeager, E. B. et al. and they found that the ORR activity of Pt surfaces increases in the order of (110) > (111) > (100) within the potential range of −0.07 to 0.8 V (vs. RHE) [17]. According to the above-mentioned d-band theory, ε_d is dependent on the CN. The average CN of surface Pt atoms is listed in the following order: (110) < (100) < (111), and ε_d, O-adsorption energy, varies accordingly. The higher ORR performance of (110) face was caused by the surface reconstruction that occurred during the reaction. For the unreconstructed (110), the activity was lower than (111) [18]. Therefore, understanding the structural factor, especially the key role of surface geometry playing in ORR, is of significance.

2.1.2 *Ligand effect*

The ligand effect refers to the Pt atoms on the surface can be regulated by the surrounding foreign atoms in an alloy system. For example, density functional theory (DFT) results studied by Kitchin et al. indicated that the energy of ε_d on Pt surface can be decreased by interacting with diverse subsurface 3d metals, such as the transition metal from Ni to Ti in the periodic table [19]. This phenomenon was also confirmed by ultraviolet photoemission spectroscopy (UPS) for Pt_3M (M = Ni, Co, Fe, V, and Ti) experimentally [20, 21]. Afterwards, it was demonstrated that the ligand effect was also related to the amount of transition metal atoms. For example, the specific activity showed a volcano-shaped relationship with the increasing amount of Cu atom at the sub-surface [22].

2.1.3 *Strain effect*

The difference of lattice constants between surface Pt and the neighboring crystal structure results in the strain effect. Briefly, the expanded strain on Pt surface, which comes from the increase distance between surface Pt atoms, can cause stronger O-adsorption. On the contrary, the O-adsorption can be weakened by the compressive strain [23–25].

The above theory provides valuable information to design highly efficient Pt-based catalysts and numerous robust Pt-based catalysts have developed. The typical example was reported in 2016 by X. Duan et al., and the one-dimensional (1D) jagged Pt nanowires (J-PtNWs, Fig. 3(a)) achieved the highest ORR activity (an electrochemical active surface area (ECSA) of 118 $m^2 \cdot g_{Pt}^{-1}$ and specific activity (SA) of 11.5 $mA \cdot cm^{-2}$ at 0.9 V vs. RHE), which is more than 50 times higher than the commercial Pt/C catalyst [26]. Besides, based on the mass activity (MA) Tafel plot, the J-PtNWs demonstrated 30 times higher MA than the 2017 target of U.S. Department of Energy (DOE) (0.44 $A \cdot mg_{Pt}^{-1}$ at 0.90 V for MEA). Experimental and DFT results show the improved ORR activity is derived from the under-coordinated surface atoms (coordination number ranges between 6 and 8), and highly stressed and rhombus-rich surface. In this way, the surface-active sites can be effectively improved and the binding energy of the surface adsorbent can be reduced.

Considering practical application, lowing the catalyst cost by increasing the Pt utilization efficiency or decreasing the amount of Pt utilization is highly demanded. Alloying Pt with other metals or designing core–shell structure has been confirmed to be the effective strategy. Meanwhile, the chemical environment of Pt atoms, such as coordination environment and catalytic surface, can be optimized by this method. For example, Pt-Pd alloys and Pd@Pt core–shell structures have been widely studied due to their suitable lattice matching and the ORR activity can be efficiently enhanced by modulating the Pt/Pd ratio and the facet structure [27]. Reactive molecular dynamics simulations indicate that the oxygen adsorption energy can be decreased at the compressed Pt surfaces, which is induced by the coexistence of Pd. However, the high cost of Pd is still a stumbling block for its wide spread. To decrease the contents of Pt or Pd and increase the metal atom utilization efficiency, nanocage structures are designed and investigated subsequently. As an example, under optimized conditions, the hollow Pt-Pd (Pd 6.4 wt.%) nanocages could achieve higher ORR activity compared with Pd@Pt (Pd 66.1 wt.%) solid nanoparticles. The specific ECSAs values of 46.8 and 38.2 square meters per gram of Pt ($m^2 \cdot g_{Pt}^{-1}$) were achieved for cubic and octahedral nanocages, respectively, which were comparable with the value of the Pt/C catalyst (56.8 $m^2 \cdot g_{Pt}^{-1}$), even though the size of Pt-Pd nanocage was much higher than the Pt NPs in Pt/C catalyst (~ 20 vs. 2.8 nm). Besides, the octahedral nanocages showed a mass activity of 0.75 $A \cdot mg_{Pt}^{-1}$ at 0.9 V (vs. RHE), which was five times higher than the value of Pt/C (0.14 $A \cdot mg_{Pt}^{-1}$) and also greater than the 2017 target of U.S. DOE (0.44 $A \cdot mg_{Pt}^{-1}$ at 0.90 V for MEA). Considering the practical application, the Pt octahedral nanocages also exhibited decent long-term stability. The MA and ECSA were dropped only 36% and 23%, respectively, after 10,000 cycles. These values were still much

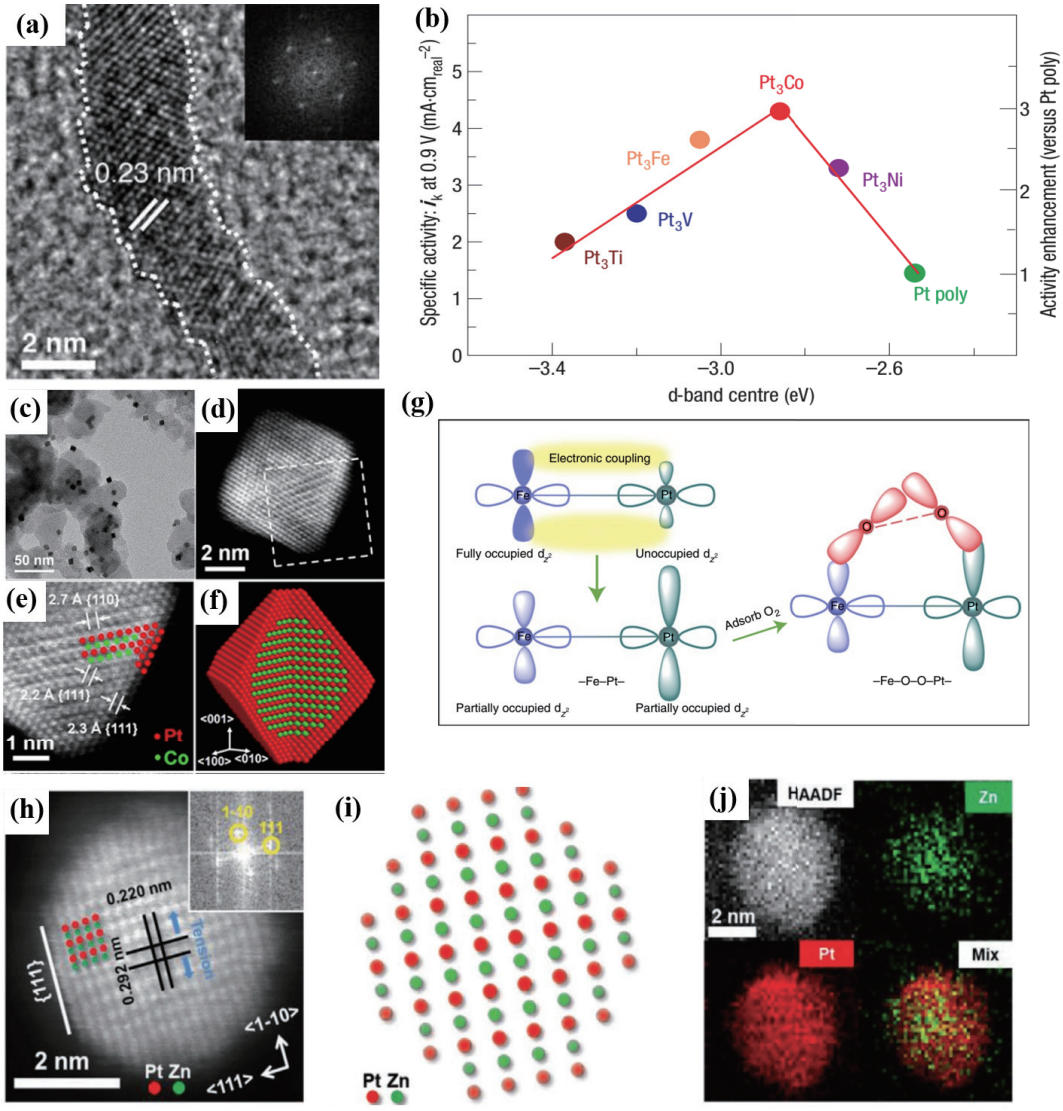

Figure 3 (a) High-resolution transmission electron microscopy (HRTEM) images of the 1D jagged Pt nanowires supported on carbon. Reproduced with permission from Ref. [26], © The American Association for the Advancement of Science 2016. (b) The relationships between the d-band centre position and the ORR performance on Pt_3M surfaces at 0.9 V. Reproduced with permission from Ref. [44], © Nature Publishing Group 2007. (c) Transmission electron microscopy (TEM) image of the obtained fct-Pt-Co@Pt octahedral nanocrystals supported on carbon. (d) High-angle annular dark-field scanning transmission electron microscopy (HAADF-STEM) images for a nanoparticle. (e) Atomic-resolution STEM image selected from (d). (f) Schematic of the nanoparticle featuring the configuration of the Pt (red) and Co (green) atoms. Reproduced with permission from Ref. [46], © American Chemical Society 2021. (g) The schematic diagram of Pt–Fe electronic coupling effect for O_2 activation. Reproduced with permission from Ref. [47], © Gao, R. J. et al. 2021. (h) HAADF-STEM image (inset: the fast Fourier transform (FFT) pattern), (i) standard atomic arrangement from the $11\bar{2}$ direction, and (j) the corresponding elemental mappings of Pt and Zn for a $L1_0$-PtZn nanoparticle. Reproduced with permission from Ref. [49], © WILEY-VCH Verlag GmbH & Co. KGaA, Weinheim 2020.

higher than the pristine Pt/C, indicating the potential application in fuel cells. Combined with DFT and experimental results, the enhanced ORR performance is due to the increased active sites and the shortened Pt–Pt interatomic distance [28].

Another effective strategy to decrease the cost of Pt-based catalysts is introducing non-noble metals. Alloy catalysts containing lower percentage of Pt not only inherit the merits of the Pt constituent but also usually demonstrate an improved performance compared with monometallic Pt [29, 30]. Over the past decades, various Pt-based alloy catalysts, such as PtCu, PtFe, PtNi, PtCo, and PtW, have been explored [31–43]. As early in 2007, Stamenkovic et al. have investigated the roles of 3d metals in the Pt_3M alloys (M = Ni, Co, Fe, and Ti). As shown in Fig. 3(b), the results indicated the ORR activities (in 0.1 M $HClO_4$ at 333 K) have a "volcano-type" relationship between the surface electronic structures (the d-band center) [44]. It seems that the Ni, Co, and Fe are the preferred alloying elements with Pt. For example, in 2007, it has been reported by V. R. Stamenkovic et al. that the specific activity of Pt_3Ni (111) surface can reach up to 10 times higher than the corresponding Pt (111) surface and 90 times higher than traditional Pt/C catalysts (~ 0.2 mA·cm^{-2} at 0.9 V vs. RHE when the paper published) for PEMFC [29]. In addition, The ORR activity of the well-designed Pt_3Ni nanoframe with open architecture can reach up to that of polyhedra structure. Due to the advantage of the well-designed structure, the reactants can be more easily accessed on both internal and external surfaces and the electronic structure on the surface Pt atoms could weaken the oxygen binding energy. The mass activity (5.7 A·mg$_{Pt}^{-1}$ at 0.9 V vs. RHE) was more than an order of magnitude higher than the 2017 target of the U.S. DOE (0.44 A·mg$_{Pt}^{-1}$) [45]. Y. Xia et al. successfully obtained a robust ORR catalyst of fct-Pt-Co@Pt intermetallic nanocrystals with {111} facets as the dominant facets (Figs. 3(c)–3(f)). The mass and specific activities could reach up to 2.82 A·mg$_{Pt}^{-1}$ and 9.16 mA·cm^{-2}, which are 13.4 and 29.5 folds higher than the commercial Pt/C catalyst, respectively. The value of mass activity was also greater than the 2025 target set by the

U.S. DOE (0.44 A·mg^{-1} at 0.9 V vs. RHE). More importantly, because of the enhanced metal–support interaction and well dispersed nanoparticles, the mass activity only dropped 21% after 30,000 cycles of accelerated durability test (ADT), indicating the promising application potential [46]. Very recently, J. Zou et al. constructed a Pt/Fe_2O_3 hybrid with dispersed Pt–Fe pair site, which overcomes the weakness of single-site Pt. The mass activity was calculated to 14.9 A·mg$_{Pt}^{-1}$ (at 0.95 V vs. RHE) and no obvious activity decay was detected after 50,000 cycles. Besides, according to the specific energy density and Pt utilization efficiency, it also exhibited enhanced performance than 20% Pt/C in a H_2-O_2 fuel cell. It is proposed that the electronic coupling effect existed in Pt–Fe pairs leads to the partially occupied orbitals and optimized oxygen binding strength. The O_2 can be adsorbed on the Pt–Fe pairs cooperatively with the O=O bond dissociation (Fig. 3(g)). Meanwhile, the OH* can desorb from the Pt site [47]. Another exciting example is the PtCo alloy, which has been successfully applied in the Toyota MIRAI fuel cell vehicle (FCV). The ORR activity in the MIRAI has been improved 1.8-fold compared with the 2008 FCV model which used Pt as ORR catalyst by regulating the composition of the PtCo catalyst [48]. Except Fe, Co, and Ni, Zn has also been investigated as a potential metal to alloy with Pt due to its advantage of antioxidant in Fenton reaction. In 2020, Q. Li et al. successfully synthesized ultrasmall $L1_0$-PtZn NPs with a "Pt-skin" structure by using a three-dimensional (3D) Pt@ZnO matrix as precursor (Figs. 3(h)–3(j)). This well-designed ORR catalyst demonstrated both excellent activity (0.52 A·mg$_{Pt}^{-1}$ at 0.9 $V_{iR\text{-free}}$; $V_{iR\text{-free}}$ indicates the voltage of the fuel cell where the internal resistance is compensated) and stability (16.6% loss in mass activity after 30,000 cycles) in PEMFC tests, outperforming the U.S. DOE 2020 targets. It was proposed that the optimized surface Pt–Pt distances and Pt–O binding account for the enhanced activity and the increased vacancy formation energy of Zn atoms leads to the increased stability [49]. In addition to the Pt-riched alloys, Chen et al. also studied the Pt-enriched alloys. The PtW_2 alloys demonstrated both higher mass activity (nearly four times increase) and stability than the Pt/C, demonstrating the great potential to solving the catalyst issues in existing PEMFCs [50]. Except Pt alloys, the Pd is another classic Pt group metal that can be used as efficient ORR catalyst. For example, S. Guo et al. successfully obtained a Pd-Mo alloy nanosheet with abundant electrochemically active sites and highly atomic utilization. The mass activity (16.37 A·mg$_{PGMs}^{-1}$) is 78 and 327 times higher than those of commercial Pt/C and Pd/C, respectively, in 0.1 M KOH. It was concluded that the improved ORR performance derived from the alloying, strain, and quantum size effect, among which the alloying effect played the key role [51]. Moreover, it also showed enhanced mass activity (0.66 A·mg$_{PGMs}^{-1}$ at 0.9 V vs. RHE) than the commercial Pt/C and Pd/C in acid solution, and higher than the 2020 technical target set by the U.S. DOE (0.44 A·mg$_{PGMs}^{-1}$), however, the stability is insufficient for practical applications and needs further effort.

2.2 Non-PGM catalysts

According to the cost analysis of PEMFCs, the Pt catalysts are responsible for more than half of the fuel cell stack and ~ 23% of the fuel cell's cost, respectively. Since the catalysts at both anode and cathode are all based on Pt or Pt alloys practically, both should be substituted by low-cost catalysts ideally. Whereas, the ORR requires more Pt than the faster H_2 oxidation reaction at the anode, therefore, lowing the cost of ORR catalysts is the urgent demand to the broad dissemination of this clean energy technology. According to the latest target set by the U.S. DOE, the ORR activity should reach 44 mA·cm^{-2} at 0.90 V, with 1.0 bar H_2 and O_2 for PGM-free PEMFC cathodes by 2025 [52]. Therefore, the central task is developing low-cost catalysts with high activity and durability. Over past decades, remarkable improvement in catalytic performance has been achieved [53]. In this section, we mainly talk about the transition metal compounds, such as metal oxides, carbides, nitrides, phosphides, and chalcogenides. To optimize the ORR performance of the transition metal catalysts, electronic structure regulation, defect engineering, and introducing supports are the widely accepted strategies.

2.2.1 *Transition metal-nitrogen-carbon (MNC) catalysts*

It is widely accepted that the MNC catalysts are the most promising candidates to replace Pt because of their merits of high activity, stability, and low cost. Since the early work conducted by Jasinski [54] and Yeager et al. [55], various MNC materials have been developed as ORR catalysts and achieved great progress. Although the catalytic mechanism and active sites of MNC catalysts are still controversial, their catalytic performances have a close relationship with (a) the types of nitrogen and metal precursors; (b) the elemental composition and interactions between different components; (c) specific surface area; (d) synthesis conditions, such as heat treatment temperature; and (e) support substrates. To obtain MNCs, the nitrogen-containing organic polymers, such as polyaniline, melamine, and polydopamine, are usually used as the N, C precursors to obtain effective MNC catalysts [56–60].

In 2011, Zelenay et al. successfully obtained polyaniline-FeCo-C and the 700-h stability test at a constant fuel cell voltage of 0.4 V (2.8 bar H_2/2.8 bar air; 0.25 mg·cm$_{Pt}^{-2}$; and work temperature 80 °C) demonstrated its promising application at the fuel cell cathode [61]. For the MNC ORR catalysts, the low active site density and low utilization sites are the two major challenges to further optimize the catalytic activity. To overcome the above obstacles, Xu et al. designed Fe-N-C SACs with a high density of active sites and efficient mass transport (Fig. 4(a)). When applied in PEMFCs, the high current densities of 0.022 and 0.047 A·cm^{-2} at 0.9 and 0.88 $V_{iR\text{-free}}$, respectively, can be achieved [62]. Very recently, Q. Jia et al. introduced a chemical vapour deposition (CVD) method to synthesize Fe-N-C ORR catalysts by flowing Fe^{3+} vapour over a Zn-N-C matrix at 750 °C. By this way, the gas-phase and electrochemically accessible Fe-N_4 active sites with 100% utilization are formed and the final catalyst demonstrated an excellent ORR activity of 33 mA·cm^{-2} at 0.90 V in a H_2-O_2 fuel cell at 1.0 bar (80 °C) [63]. Recently, J. Yang and Y. Jiang et al. designed the iron-nitrogen/carbon (Fe-N_x/C) catalyst by a pyrolysis strategy. The highly graphitized N-doped carbon substrate can effectively stabilize the isolated Fe-N_x sites and improve the antioxidant ability of the Fe-N_x/C catalyst. Under optimized conditions, the half-wave potential ($E_{1/2}$) can reach to 0.811 V (vs. RHE in acid media) and the stability can sustain for 30,000 cycles with only 25 mV loss of $E_{1/2}$. When applied in a fuel cell, the power density can reach 656 mW·cm^{-2} and 71% current density can retain after 100 h of test at a voltage of 0.5 V [64]. It should be noticed that although the Fe-N-C catalysts demonstrated promising ORR electrocatalytic efficiency, the poor stability in PEMFCs is the main challenge that limited its wide application. It is because the Fe ions can react with the byproduct of H_2O_2 (Fenton reactions) and generate highly reactive hydroxyl and hydroperoxyl radicals, which then induce the degradation of ionomers and membranes [65–67]. By contrast, Co-N-C SACs seem to be a promising alternative due to the less undesired Fenton effects. However, Co-N-C SACs demonstrate inferior ORR electrocatalytic activity [68]. Therefore, improving the catalytic efficiency is the direction of effort. For example, He et al. prepared Co-N-C SACs by a surfactant assisted confinement strategy and obtained abundant active Co-N-C sites on the edge of carbon layers [69]. Through this strategy, the performance of the catalyst can be comparable to that of typical Fe-N-C SACs.

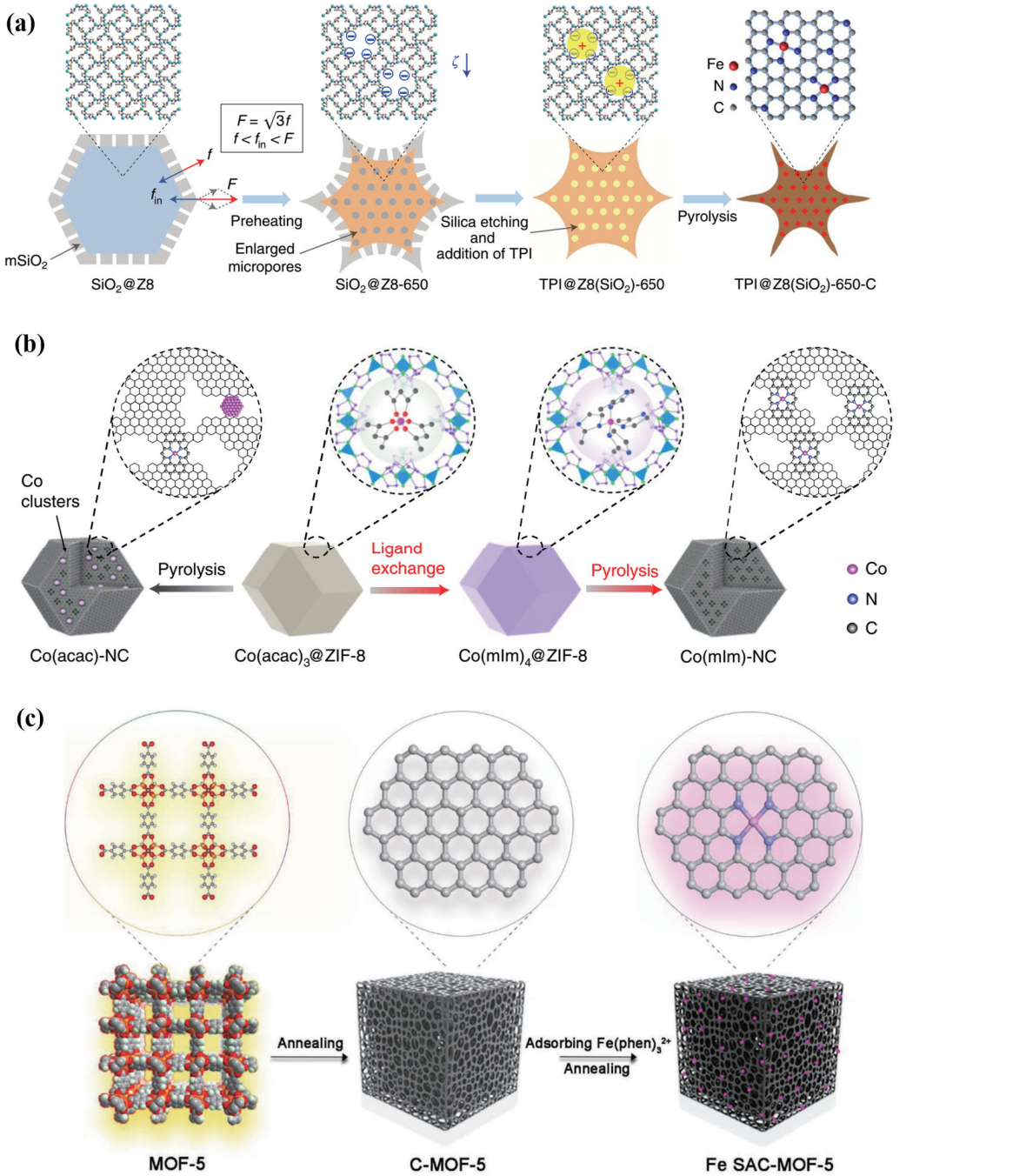

Figure 4 (a) The synthesis method of Fe-N-C SACs (triple 1,10-phenanthroline (phen) iron (TPI)@Z8(SiO_2)-650-C) derived from TPI and ZIF-8. Reproduced with permission from Ref. [62], © Wan, X. et al. 2019. (b) The synthesis procedure of the atomically dispersed Co-N-C catalyst. Reproduced with permission from Ref. [70], © Springer Nature, 2019. (c) The scheme of synthesis method for the Fe SAC-MOF-5 catalyst. Reproduced with permission from Ref. [103], © Wiley-VCH GmbH 2021.

Recently, Y. Shao et al. reported an atomically dispersed Co-N-C ORR catalyst by immobilizing the ligand-chelated CoN_x in the micropores of zeolitic imidazolate framework (ZIF)-8 rather than by an ion exchange method (Fig. 4(b)). It reached up a current density of 0.022 A·cm^{-2} at 0.9 $V_{iR\text{-free}}$ with an enhanced durability compared with that of Fe-N-C catalyst. A peak power density of 0.64 W·cm^{-2} in 1.0 bar H_2/O_2 fuel cells was achieved, which is the highest value among the reported non-Fe and Pt-metal-free catalysts when it was published. The improved durability is due to the lower activity for Fenton reactions and increases the resistance to demetallation of Co-N-C [70]. In addition to inferior catalytic activity, the undesired 2e$^-$ ORR pathway in acidic media to produce H_2O_2 is another disadvantage that should be improved for Co-N-C SACs [71]. It is speculated that the high activation energy for O–O bond breaking and the weak adsorption between H_2O_2 and the Co-N_4 active sites lead to the 2e$^-$ ORR pathway [72]. Furthermore, the poor stability in acid media also greatly limited its wide application [73]. To improve the stability of M-N-C SACs, alternative metals besides Co and Fe can be selected in practical PEMFCs. Mn-N-C SACs demonstrated improved stability than Fe-N-C and Co-N-C SACs since the Fenton reaction and 2e$^-$ ORR pathway can be effectively restrained by the Mn-N-C active sites. Whereas, the ORR activities are inferior to those of Fe-N-C and Co-N-C catalysts [74–77]. Apart from Fe, Co, and Mn, other metals such as Cu [78], Zn [79], Cr [80], and W [81] have also used as M-N-C ORR SACs. Based on the above analysis, the developed M-N-C SACs are promising ORR catalysts to replace noble metals, however, each of them has different disadvantages to achieve practical application. To further improve their performance, deep mechanistic investigations are necessary [82].

2.2.2 Transition metal oxides (TMOs)

Manganese and cobalt oxides are the two kinds of popular transition metal oxides catalysts. The previous results have demonstrated that MnO_x can serve as an effective catalyst to translate HO_2^- to H_2O by a 4-electron transfer process [83, 84]. Nevertheless, the poor electrical conductivity of metal oxides seriously limits their application in fuel cells. To overcome this obstacle, the substrates with high conductivity, such as carbonaceous materials, are usually introduced to support the metal oxides. For example, Z. Yang et al. reported the MnO_x/carbon nanotubes catalyst with enhanced ORR activity and stability, which are comparable to Pt/C catalyst [85]. This strategy is also suitable for cobalt-based oxides. When combined with graphene or carbon nanotubes, the ORR activity of cobalt oxides (such as Co_3O_4 and CoO) can be drastically enhanced [86, 87]. It should be noted that not all carbon materials have a positive synergistic promotion effect, which depends on coupling model between the oxide nanoparticles and the carbon support. Some reported studies found that the strongly coupled carbon nanotube materials demonstrate a higher ORR activity than the graphene counterpart [87].

2.2.3 Transition metal carbides (TMCs)

With the merit of good conductivity, TMCs have been applied in various catalytic reactions. However, they show poor stability in acid medium and well-designed decoration should be considered when used as catalysts in ORR. Generally, carbon materials are usually introduced as wrappage for TMCs to resist the acid conditions. At the same time, this strategy can also avoid the sintering of the TMCs nanoparticles. In 2018, S. Guo et al. reported the well-designed PtFe-Fe_2C Janus-like nanoparticles, which exhibited much higher ORR catalytic performance than PtFe and Fe_2C NPs in either acidic and alkaline electrolytes. DFT results indicated that electron transfer exists on the interface of the hybrid and leads to the excellent ORR performance [88]. Guo et al. encapsulated the WC nanoparticles in the graphitic layers (WC@C) with a mean diameter of only 1.9 ± 0.9 nm, which not only increases the conductivity but also improves the stability by avoiding the coarsening of WC [89]. Similarly, Xiao et al. obtained Fe_3C@N-graphene oxide (GO) catalysts with high ORR performance and durability in both acidic and alkaline conditions [90]. Although TMCs have received much attention, it is still difficult to identify the exact composition that plays the active catalyst in the TMCs, because the composition in the TMCs is very complicated and they usually consist of different metal valence. For instance, the tungsten carbide might be composed of WC and W_2C. In addition, the N element in the substrate might affect the active sites of TMCs. Therefore, further study is need to investigate the roles of each component in ORR mechanism and then provides significant information to explore more active TMCs catalyst.

2.2.4 Transition metal nitrides (TMNs)

Generally, the TMNs possess better corrosion resistance and conductivity than those of metal oxides. However, the ORR activities for most of TMNs cannot compare to Pt/C. Over the past decades, great effects have been made to improve their ORR performance. It is found that the doping engineering is an effective strategy. For instance, by introducing Ni as a doping element into the TiN nanoparticles, the ORR performance can be improved remarkably and even can be comparable to that of Pt/C in alkaline electrolytes [91]. It is proposed that the electron transfer between Ti atoms and adsorbed oxygen molecules can be promoted by Ni doping. Besides, the structure optimization is another method to improve the ORR activity. In 2018, S. Liao and B. Y. Xia et al. successfully obtained $Ti_{0.8}Co_{0.2}N$ nanotubes, which exhibited much higher ORR performance compared with the nanoparticle in the full-cell level [92]. The enhanced ORR may be due to the large surface area of the hierarchical architectures. In addition, coupling TMNs with porous carbon supports can also optimize the ORR activity. For instance, the ORR performance of $FeCoN_x$ can be dramatically enhanced when combined with the hierarchically porous carbon cages. It was speculated that the synergetic effects between Fe and Co element and unique superstructure lead to the remarkable electrocatalytic performance [93].

2.2.5 Transition metal phosphides (TMPs)

Due to the distinct merits, such as tunable structure and unique physicochemical properties, TMPs have provided new opportunities to design efficient and durable low-cost ORR catalysts in acidic solutions. Different metals or stoichiometric ratios of metal/phosphorus can lead to various compounds with diverse structure and physicochemical characteristics. In general, the TMPs with abundant M–M bonds and M–P bonds possess better electron conductivity and stability than that of the P-rich TMPs with more P–P bonds. In 2015, Yu et al. first introduced Fe-P-C as ORR catalyst experimentally [94]. After that, a series of TMPs with comparable activity and durability have emerged. However, the ORR performance is still inferior when compared with Pt/C catalysts. To improve the performance, Q. Xu et al. recently designed an efficient and stable Co_2P ORR catalyst by embedding in Co, N, and P multi-doped carbon. Due to the synergistic effects between the multi factors, the ORR activity can be comparable to that of Pt/C [95]. Furthermore, C. Hou and co-workers immobilized the ultrafine CoP_x NPs on two-dimensional (2D) carbon nanosheets on nickel foam with porous 3D interconnected network. The obtained self-supported electrodes demonstrated remarkable catalytic ORR properties with an onset potential of 0.83 V (vs. RHE) and a $E_{1/2}$ of 0.76 V (vs. RHE) [96].

2.2.6 Transition metal sulfides (TMSs)

Compared with other low-cost ORR catalysts, TMSs have received less attention because of their poor activity and low electrical conductivity. To optimize their performance, several efforts have been taken. For example, Zhang et al. designed and synthesized a hydrosulfide of $Co_3FeS_{1.5}(OH)_6$ with preserved morphology, which demonstrated excellent ORR activity in alkaline media [97]. Another work is the N-doped Co_9S_8/graphene composite. Due to the N doping and the formed rich defects and active sites, it showed outstanding ORR activity and durability in alkaline media [98].

2.3 C-based catalysts

C-based materials, such as carbon nanotubes, graphenes, and carbons derived from metal-organic frameworks (MOFs), have been widely applied in designing efficient ORR electrocatalysts. They usually can be used by combining with the metal-based catalysts. Generally, a positive synergistic effect can be induced between the doped metal and the adjacent carbon atoms, which can promote charge redistribution and then improve the electrocatalytic activity. It is widely accepted that the formed metal-N_4 chelate bonds for the transition metal-doped C catalysts and the *ortho*-C atoms of the pyridinic ring for C catalysts are the ORR-active sites.

Since not all the "active sites" in C-based catalysts can play their roles at the RDE level, improving the utilization efficiency of active sites has attracted sustainable attention. To get more electrochemically inaccessible active sites, designing hierarchically

porous structures is an effective strategy. For example, Z. Bai et al. reported a 3D Fe-N-C ORR electrocatalyst by the structural arrangement of ZIF-8 nanograins and the results revealed that the abundant and multiscale macro-sized pore channels played the main role to promote the intrinsic catalytic efficiency [99]. Due to the merits of the coexistence of abundant C, N, and metal elements, MOFs have become hot materials to synthesize C-based ORR materials. Xia et al. successfully got the hollow structure of Co/N-doped CNTs by using ZIF-67 as the precursor and the ORR efficiency was enhanced clearly because of the highly porous hollow carbon matrix [100].

2.4 SACs

To maximize the atomic utilization and increase the catalytic performance, SACs electrocatalysts have attracted extensive interest. For SACs, the metal active sites are highly dispersed on the substrate at the atomic level. Therefore, it is a promising strategy to reduce the usage of metals, especially the noble metals. Although the usage of metals is decreased, the ORR performance of SACs can maintain or even surpass the counterparts in other motifs (e.g., metal nanoparticles and clusters), which is of great significance for reducing the cost of catalysts. More importantly, the demetallation issue that widely existed in the C-based catalysts can be optimized by the SACs strategy. At the same time, because of the strong interaction between the metal atoms and the substrate, the stability can also be improved. For example, Li et al. successfully obtained Co-based SACs using the Co/Zn MOF as precursor. Under high reaction temperature (> 800 °C), the Zn metals were evaporated, while the Co element was retained in the carbon substrate and Co-N_x single sites were formed, which showed excellent ORR performance [101]. Similarly, the Ni SACs can be obtained from Ni NPs under high-temperature reaction conditions. It is speculated that the strong interaction between Ni atoms and the N atoms on the surface of the matrix can be gradually drawn away from Ni NPs [101]. Recently, Q. Xu et al. reported the robust single Fe sites by a silica-mediated MOF-templated method, which demonstrated excellent ORR performance and stability in both acidic and alkaline solution, which even can comparable to those of Pt/C catalysts. It is speculated that the overhang-eave morphology benefits for the mass transport and active metal site utilization [102]. T. Zhang et al. developed a Fe SAC supported on Zn_4O(1,4-benzenedicarboxylate)$_3$ (MOF-5)-derived carbon with outstanding hierarchical porosity and abundant accessible FeN_x sites (up to 2.35 wt.%). A high halfwave potential of 0.83 V (vs. RHE) was achieved in acid electrolyte and the peak power density can boost to 0.84 W·cm^{-2} in H_2-O_2 PEMFC (0.2 MPa) (Fig. 4(c)) [103]. The intrinsic ORR efficiency of SACs can be further enhanced by optimizing the coordination environment and improving the amounts of active sites.

3 ORR catalysts applied in MEA or fuel cell

Based on the ORR activity of the reported works, it seems that the ORR performance is not the challenge to construct a hydrogen fuel cell with high efficiency. However, most of the results are just at RDE level and there are relatively few results available for the investigations in practical MEA and fuel cell applications. The major differences between RDE and MEA level are as follows: (i) Mass transfer resistance can be largely eliminated on the RDE level because of the high-speed rotating; however, it cannot be overlooked in the practical MEA and fuel cells. The typical example is the nanoframe catalysts, for which the mass transfer of protons to the inner surface has not been a problem in RDE test. Whereas, it becomes a great challenge in MEA application since the ionomer is difficult to penetrate into the pores that are less than 20 nm and proton transport is greatly limited at moderate to high current densities. Then it results in the poor catalyst utilization [104]. (ii) Catalyst layer. The active sites of the catalysts can be used to the maximum extent on RDE level, whereas, because of the triple-access (gas–liquid–solid) reaction conditions, it is a great challenge to reach the similar utilization efficiency at the MEA level. In MEA application, the catalyst layers are 5–20 μm, which are much thicker than in RDE test (0.1–2 μm), and the contact between the reactants and catalyst layer becomes more difficult at the three-phase zones (the polymer electrolyte, the solid catalysts, and the oxygen gas). The thin-film electrode can reach 100% utilization of the catalyst in a RDE, whereas, it is difficult to achieve such high value at MEA level, because of the essential difficulties of triple-access requirement and dynamic challenges from water flooding. Besides, conductivity influence is negligible in RDE due to the low film thickness, however, it cannot be ignored at the macroscopic MEA level. Reducing the catalyst layer, such as removing the carbon substrate, is the direction of efforts. It is because the thinner catalyst layer can provide improved heat and water transport, and shorter mass and electron pathway, and then increase the utilization of the catalyst at all current densities [105]. (iii) The concentration of O_2 is much lower for RDE tests than that of MEA tests. Although conducted at high rotation rates, the O_2 concentration is strongly limited in the liquid electrolyte for RDE tests, whereas, MEA tests are measured at O_2/air atmosphere. To achieve the same Pt-specific current density, the RDE test requires lower catalyst loading (< 0.5 μg·cm^{-2}) on the electrode disk. With such low catalyst loading, it is difficult to deposit them as a homogeneous film and the performance can be easily influenced by the impurities, leading to the challenges of experimental reproducibility. (iv) The test system of MEA cell is much more complicated than that of RDE. The MEA mainly consists of gas diffusion layer (GDL), catalyst layer, and proton (ion) exchange membrane. Usually, the GDL is compressed by the contact pressure between the rib and the GDL, which leads to the thinner portion of the GDL and higher water saturation. Then, the remained water in the GDL leads to compromised oxygen transport and non-uniform power generation. To overcome this issue, a 3D mesh flow field has been designed in the MIRAI cell and the airflow towards the GDL and gas transport to the cathode catalyst layer can be greatly promoted [48]. (v) Operating temperature. MEA can usually be operated in the range 60–80 °C. By contrast, RDE tests are usually operated at ambient temperature because additional hardware is essential to achieve temperature control. Higher operation temperature is certainly a great challenge for the durability of the catalysts. Based on the above analysis, it is clear that the ORR activity cannot be directly translated to the MEA and fuel-cell performance. Consequently, the insufficient data on the real MEA and fuel-cell performance becomes a serious impediment for its development. Many researchers have realized the existing challenges and carried out some investigations on the MEA and fuel-cell test.

For example, Lou and Xia et al. obtained 1D bunched Pt-Ni alloy nanocages ORR catalysts [106]. Under optimized conditions, the mass activity and specific activity of $Pt_{1.5}Ni$ were 17 and 14-fold higher than the commercial Pt/C catalyst (60 wt.%, Johnson Matthey (JM)) and the stability can sustain for more than 50,000 potential-scanning cycles. When applied in a H_2-air fuel cell test, it also demonstrated an enhanced catalytic performance with a peak power and current density of 920 mW·cm^{-2} and 1.5 A·cm^2 at 0.6 V (more than 180 h), respectively, which showed a promising practical application potential. Among the Pt-M alloys measured at MEA level, the performance of Pt-Ni alloys is listed in the top-tanking, however, Ni etching is easily occurred in acid conditions

leading to the significant activity loss. Therefore, Pt-Co alloys attracted more attention. For example, Chong et al. synthesized the core–shell PtCo alloys on a PGM-free (Co-N_x-C_y) substrate using Co or bimetallic Co and Zn zeolitic imidazolate frameworks as precursors (Figs. 5(a) and 5(b)) [107]. The mass activity can reach 12.36 ± 0.53 A·mg_{Pt}^{-1} and 1.77 ± 0.39 A·mg_{Pt}^{-1} (at 0.9 V vs. RHE) tested at RDE and fuel cell level, respectively, outperforming the U.S. DOE target of 0.44 A·mg_{Pt}^{-1}. Besides, an excellent durability was also achieved no matter at high-voltage (kinetics-limited) or high-current density (mass transport-limited). It should be noticed that during the practical PEMFC operation, faster oxygen delivery and water removal are essential, however, it also promotes the diffusion of dissolved Pt atoms and the Ostwald ripening process and then accelerates the catalyst inactivation. Besides, the oxygen transport resistance in the MEA has a opposite relationship with the catalytic sites and the catalyst degradation could dramatically increase the oxygen transport resistance and activity loss. Herein, to maintain the long-term durability in PEMFCs with low Pt loading, ultrasmall size of catalysts with outstanding stability is a key issue. To overcome it, Y. Huang et al. synthesized the graphene encaged PtCo nanocatalysts (PtCo@Gnp) with both excellent mass activity (1.21 A·mg_{PGM}^{-1}) and stability (27% mass activity was lost after an accelerated durability test). It was calculated that only 6.8 g PGM was used when applicated in a 90 kW PEMFC vehicle, which is close to the usage amount in a typical catalytic converter [108].

Besides alloys, intermetallic nanoparticles have been explored as another kind of catalysts demonstrating excellent ORR performance. The merits of defined surface and near-surface atomic arrangement can effectively increase the activity and stability. For example, X. Zi et al. studied the intermetallic and ferromagnetic $L1_0$-CoPt/Pt NPs with 2 and 3 atomic layers of Pt shell and the intermetallic structures exhibited the obvious advantage in stabilizing Co and improving Pt activity for fuel cell applications [109]. Both catalytic activities can reach 2.26 and 0.56 A·mg_{Pt}^{-1} in electrolytic cell and MEA with only 18% and 19% lost at 60 and 80 °C after 30,000 cycles, respectively, which exceeded the U.S. DOE 2020 target. DFT results indicated the biaxial strain and ligand effect caused by Pt shell, and Co weakened the binding energy of the oxygenated intermediates on the surface of Pt and then improved the ORR performance. Although the atomically ordered intermetallic NPs show excellent ORR performance, the difficult synthesis is still a great challenge. It is because high temperature annealing is essential to obtain the ordering atom, however, the metal sintering also occurs during this process. To overcome this issue, H. W. Liang et al. developed a sulfur-anchoring strategy and successfully synthesized a series of Pt intermetallics (46 combinations of Pt with 16 other metal elements) with an average particle size of < 5 nm. The sintering can be effectively suppressed by the strong chemical interaction between Pt and the sulfur atoms on carbon substrate. The small nanoparticle still remained even after annealing at a high temperature up to 1,000 °C. These Pt-intermetallics (such as PtFe, PtCo, PtNi, and $PtCu_3$) also exhibited high mass activities of 1.3 to 1.8 A·mg_{Pt}^{-1} at 0.9 V (internal resistance corrected) in PEMFCs tests, which were better than the benchmark Pt/C and also higher

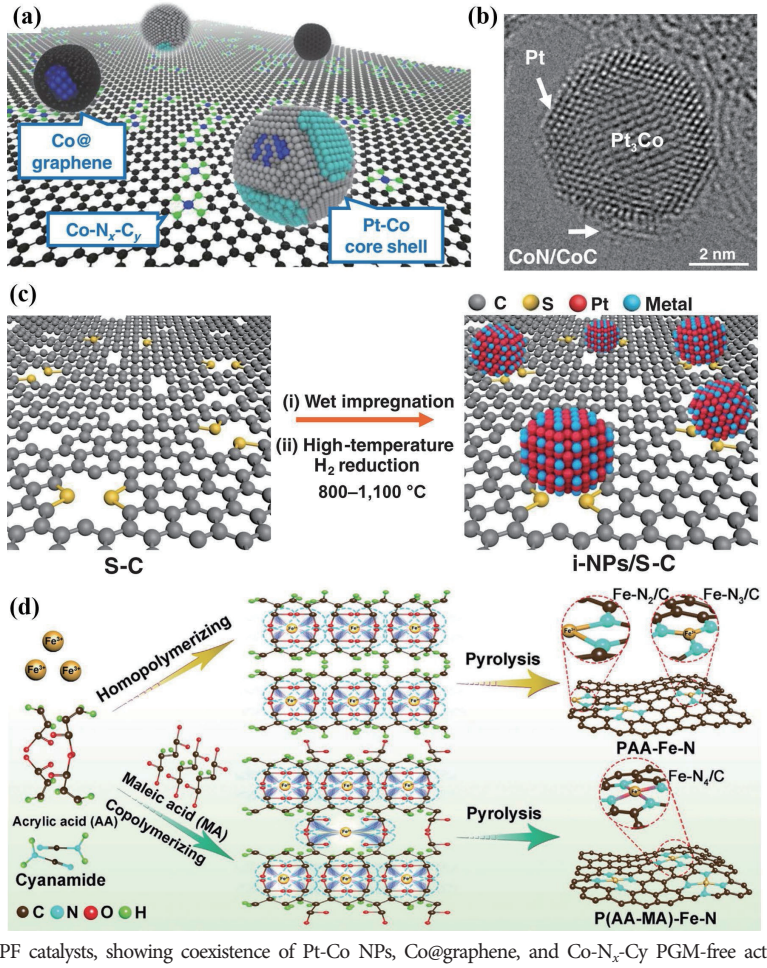

Figure 5 (a) Schematics of LP@PF catalysts, showing coexistence of Pt-Co NPs, Co@graphene, and Co-N_x-Cy PGM-free active sites. (b) HRTEM image of a representative Pt-Co alloy NP with Pt_3Co superlattice core and Pt skin partially covered by CoN and CoC terraces. Reproduced with permission from Ref. [107], © Chong, L. et al. 2018. (c) The synthesis method to obtain the Pt intermetallics. Reproduced with permission from Ref. [110], © The American Association for the Advancement of Science, 2021. (d) The preparation methods of the PAA-Fe-N and P(AA-MA)-Fe-N catalysts. Reproduced with permission from Ref. [118], © Wiley-VCH GmbH 2021.

than the U.S. DOE 2025 target of 0.44 A·mg_{Pt}^{-1} (Fig. 5(c)) [110]. Another exciting work to achieve high-load Pt intermetallics without agglomeration was reported by H. Yang et al. recently. In this work, a cobalt oxide aided structural evolution method was applied to obtain high-loaded (44.7%) core–shell Pt1Co1-intermetallic compounds@Pt/C catalyst with a quite small size of sub-6 nm. The mass activity can reach 0.53 A·mg_{Pt}^{-1} at 0.9 V (vs. RHE) on RDE level. Then, a mass activity of 0.47 A·mg_{Pt}^{-1} was calculated in the PEMFCs tests, outperforming the 2020 U. S. DOE target (0.44 A·mg_{Pt}^{-1}). More importantly, the power densities were calculated to 2.30/1.23 W·cm^{-2} for H_2-O_2/air fuel cells at 80 °C, respectively. Both experimental and theory results indicated that the lowered d-band centre and improved antioxidation of Pt/Co sites account for the enhanced activity and durability, respectively [111]. Very recently, J. N. Zhang et al. designed the concave Pt-Zn nanocubes with high-index faceted Pt skin, which possess more active surface structure and then increase the utilization of Pt. The mass activity and specific activity for Pt78-Zn22/KB were 1.18 A·mg_{Pt}^{-1} and 3.64 mA·cm^{-2} at 0.9 V (vs. RHE). In H_2-O_2 fuel cell tests, the peak power density reached up to 1,449 mW·cm^{-2}, which was higher than the commercial Pt/C [112]. In order to promote O_2 transport and increase the ORR activity, Q. Yuan et al. fabricated a (111) fact rich PtCu@PWO_x catalyst with open pores and oxygen container. Combined with the advantages of compressive strain and downshift d-band centre of Pt, the mass activity boosted to 3.94 A·mg_{Pt}^{-1}. Moreover, the power density of 218.6 and 420 mW·cm^{-2} was obtained in H_2-air and H_2-O_2 PEMFCs, which is much higher than the benchmark Pt/C, demonstrating its great potential in application [113].

Compared with the widely investigated monometallic and binary metals, the ternary or quaternary metals have received less attention at fuel cell level. Q. Yuan et al. designed a series of multi-metallic nanostructures and exhibited promising performance [114–117]. For example, in 2021, an interface-rich 3D PtBiAu intermetallic with functional sites of "Pt-Au" or "Pt-Bi" was reported. Under optimized conditions, the mass activity boosted to 28.72 A·mg_{Pt}^{-1} (8.65 times that of commercial Pt/C) and exhibited high anti-CO poisoning in direct ethylene glycol fuel cells. The peak power density can reach up to 145 and 92 mW·cm^{-2} in O_2 and air, respectively, at 80 °C [114]. Then, the 2D quaternary PdAuBiTe nanosheets were firstly synthesized and the mass activity of ORR was calculated to 2.48 A·mg_{Pd}^{-1} at 0.9 V (vs. RHE), which was 27.5 and 17.7 times that of commercial Pd/C and Pt/C, respectively. When used as cathode in the practical direct methanol fuel cell, the power density can boost to 235.7 and 173.5 mW·cm^{-2} in O_2 and air, respectively, at 80 °C, also higher than the Pt/C (101.5 and 48.3 mW·cm^{-2} in O_2 and air, respectively). It was confirmed that the topmost and edge defects, low-coordinated atoms, lattice strain, and downshifted d-band center resulted in the enhanced performance [115].

Compared with Pt-based ORR electrocatalysts, most of the non-Pt-based electrocatalysts are limited to the RDE measurements and lack of MEA data in addition to a few reports based on SACs. It is because the challenges of high operation temperature (60–80 °C and 0.5–0.8 V) in strongly acidic and humid conditions should be overcome. To suppress the demetallation of non-noble-metal M-N_x/C catalysts and increase its durability in PEMFC application, Q. Li et al. optimized the bonding strength between the metal ions and chelated polymers by regulating the ratios of acrylic acid (AA) and maleic acid (MA) in copolymer (P(AA-MA)). The bond length and coordination of Fe–N can be controlled. Under optimized conditions, the P(AA-MA)-Fe-N catalyst, which possessed abundant Fe-N_4/C sites and longer Fe–N bonds, demonstrated both outstanding mass activity and durability in half and H_2-air fuel cells. The ORR activity ($E_{1/2}$ ≈ 0.8413 V) of P(AA-MA)(5-1)-Fe-N can bear comparison with Pt/C ($E_{1/2}$ ≈ 0.841 V) and the $E_{1/2}$ only lost 6 mV after 5,000 cycles at 60 °C (Fig. 5(d)) [118]. Wan et al. synthesized a concave-shaped Fe-N-C SAC with a large external surface area and demonstrated much enhanced MEA activity as a result of the well-designed open geometric structure and improved active sites [62]. Under the U.S. DOE testing protocols, the current density can reach up to 0.047 A·cm^{-2} at 0.88 $V_{iR\text{-free}}$ (vs. RHE). A remarkable activity of 129 mA·cm^{-2} at 0.8 $V_{iR\text{-free}}$ can also be obtained under the ambient working environment (1 bar H_2-air). It is speculated that the large external surface area and mesoporosity play significant roles in exposing the Fe-N_4 active sites and enhancing the mass transport of the catalyst layer. Recently, J. Shui et al. reported a novel Fe-N-C catalyst with acid stable N-coordinated Fe clusters and Fe-N_4 active sites on 2D porous carbon for ORR in fuel cells. Both experimental and theoretically results indicated that the activity of satellite Fe-N_4 sites can be enhanced by the Fe clusters, which introduced an OH ligand and then optimized the adsorption strength of reaction intermediates and decreased the bond amplitude of Fe-N_4 by incoherent vibrations. When applied in PEMFC, the catalyst boosted the mass activity to 10 mA·mg_{cat}^{-1} at 0.9 V (vs. RHE) in acid electrolyte under 1 bar H_2-O_2 [119].

Based on the above analysis, it can be exhibited that although many of the low-cost ORR catalysts demonstrated comparable ORR performance with Pt/C at the RDE level, the catalytic performances are still inferior in contrast to those of Pt-based ORR electrocatalysts at the MEA level [11].

4 The insufficiencies of ORR electrocatalysts for practical application

4.1 Pt-based catalysts

Up to now, Pt-based catalyst is still the most efficient ORR catalyst and the performance of Pt/C is still the benchmark to evaluate other ORR catalysts. To further enhance the intrinsic activity for Pt-based catalysts, significant progress has been achieved, such as morphology and component optimization. Nevertheless, although the Pt-based ORR catalysts have been enhanced dramatically, the definite reaction mechanisms from high-index plane are still not clear. Besides, it is a great challenge to keep the well-faceted nanocrystals in the fuel cell work conditions, especially for the catalysts with high-index planes and unsaturated atomic edges, which are the active sites for ORR. During fuel-cell operation, these faces can be easily changed and deactivated, leading to the decrease of their catalytic performance and then limiting their practical application in fuel cells. For the Pt alloy catalysts containing non-noble-metals, the main challenge is the instability of non-noble metals [120, 121]. It is because in the real PEMFC application, the rigorous operation conditions (the typical operation temperature is usually at 60–80 °C and the electrolyte environment is strong acidic) lead to the oxidation and dissolution of the non-noble metals. Then, the proton exchange membrane can be degraded by the dissolved metals ions, which can react with H_2O_2, and lower the long-term performance of PEMFCs. For example, the intermetallic NPs of $L1_0$-PtFe, $L1_0$-PtCo, and $L1_0$-PtNi have demonstrated promising ORR activity and durability in PEMFCs [49]. However, the formation of reactive oxygen species (such as ·OH radical) from H_2O_2 (the main byproduct of $2e^-$ ORR) can be accelerated by these redox-active metals (especially Fe) through Fenton reaction. Subsequently, Nafion membrane and catalyst layers will be damaged by these reactive oxygen species [49].

For the commercial Pt/C catalysts, the migration, coarsening, and dissolution of the Pt NPs are the major issues that influence

the durability of the fuel cell. In practical application, the coarsening of Pt NPs proceeds via two different ways [122–124]. First, the smaller Pt NPs dissolve and subsequently redeposit on the larger Pt NPs, which is called Ostwald-ripening process. By this way, the Pt NPs can increase from ~ 3 to 6 nm on carbon. Another way is the dissolved Pt species (such as Pt^{2+}) can migrate and diffuse in the ionomer phase at the micrometer scale. These soluble Pt species can be reduced by cross-over H_2 from the anode and then form precipitated Pt NPs in the cathode ionomer phase [100]. As the Pt NPs grow, the catalytic active sites will be reduced seriously and lead to the increase of the cell overpotential, which subsequently causes the lower stack voltage at a specified current density. In addition, the dissolution of Pt can be accelerated at the high steady-state potential (0.9 to 1.1 V vs. RHE) at the real work temperature (80 °C) of PEMFCs.

4.2 Non-noble metal catalysts

Possessing the merits of abundant reserves, low cost, and easy preparation, the non-noble metal catalysts are considered as the promising candidates to replace noble metals. Whereas, there are still major challenges that should be overcame before they can be applied practically in PEMFCs. Firstly, compared with Pt/C, the unsatisfied intrinsic activities in acidic and humid conditions for most of these catalysts are the major drawbacks that limit their application. Secondly, the poor stability under PEMFC operations is another stumbling block. Thirdly, the mechanism of deactivation process for non-noble-metal catalyst is still under debate [125–127]. Specifically, each kind of non-noble metal has its own deficiency when used in MEA. For MNCs catalyst, it has been reported that the demetallation of active sites, carbon corrosion, micropore flooding, and protonation of the N-groups on the surface are the possible reasons that lead to the performance degradation. For the highly active Fe-N-C catalysts, the first two factors are the major reasons leading to the obvious degradation of the catalytic activity. Besides, the leached Fe ions could react with the hydrogen peroxide generated during ORR and then the produced hydroxyl radicals would damage the carbon matrix, ionomer, and proton exchange membrane. For TMOs catalyst, the poor electrical conductivity and instability in strongly acidic environments seriously limit their practical application in fuel cells. Carbonaceous materials are essential to be used as the substrates or wrappages to optimize their conductivity and stability, which significantly increases the difficulty of catalyst design and large-scale synthesis. For TMNs, although many reported works have demonstrated their better corrosion resistance and conductivity than those of metal oxides due to the stable triple bonds between metal and N atoms, most of the intrinsic activities still have a great distance compared with Pt/C even at the RDE level. For TMCs, although with the merit of good conductivity, poor stability in acid medium is the major challenge in MEA. Similar with TMOs, carbon and/or graphitic layers are the widely used material to encapsulate the catalysts. However, it increases the complexity of the component at the same time, which then influences the repeatability of the performance. For example, the type of N and its related content in carbon materials would have a close relationship with the activity, whereas, it is a great challenge to keep the same for different batches of catalysts. Apart from that, it is still a great challenge to identify the exact catalytic active sites and the detailed structures of the active sites. For TMPs and TMSs, designing active and stable catalysts in acidic electrolytes is the pivotal challenge, since their ORR performance is still much more inferior compared with the benchmark Pt/C. Based on the above analysis, each kind of non-noble metal has its own deficiency for MEA application. Besides, the available data on the MEA tests for the non-noble metal ORR catalysts is still insufficient at present. Herein, there is still a long way to reach a comparable activity and stability with Pt/C catalyst [11].

4.3 C-based catalysts

The major challenge for the practical application of C-based ORR catalysts is the demetallation and carbon corrosion. Especially, under high-electrode potentials and transient conditions, the performances become even worse [128]. To overcome this issue, encapsulating the metal by carbon shell is an effective method. Whereas, the active sites are reduced at the same time. In addition, increasing the graphitization is another widely used strategy, whereas, the highly graphitized carbon configurations are undesirable to anchor the active sites, such as $M\text{-}N_4$. In practical application, carbon corrosion easily occurs when the anode is at a high electrode potential state (such as 1.3 V vs. RHE) due to the hydrogen starvation. The decreased activity of fuel cell derived from of carbon support damage is irreversible. To avoid the high electrode potentials, a cell voltage monitor (CVM) system is usually introduced. Whereas, it is too expensive and does not benefit for the popularizing of fuel cells. To avoid the use of CVM system, it is urgent to develop a durable substrate material to replace carbon.

4.4 Single-atom metal catalysts

As mentioned above, the synthetic processes for the SACs are usually rigorous, which needs precise reaction temperature and sophisticated precursors. Therefore, high costs are inevitable to obtain SACs with high quality and it is a great challenge to achieve large scale production. Furthermore, to avoid aggregation and sintering, the weight percentages of the loaded metals are usually very low (< 1 wt.%), which leads to the low amounts of available active sites [129–130]. In addition, most of the performance evaluation for the SACs is conducted at RDE level and the further measurements on the MEA or fuel cell level are urgently demanded.

5 Perspectives and conclusions

5.1 Design more sufficient ORR catalysts

Although the synthesis of Pt/C catalysts has achieved industrial-scale production, further lowering the preparation cost may be an effective way to decrease the price of fuel cell and expand its practical application. For low-cost ORR electrocatalysts, it is necessary to increase both ORR activity and stability. Various strategies have been developed, such as morphology modification and phase optimizing [131]. One encouraging case is that one kind of noble-metal-free ORR catalysts has been applied in the fuel cell in 2017 by Ballard Power Systems. Therefore, it can be predicted that the low-cost catalyst will play the lead in the future with the sustained efforts from both basic and application research (Ballard news releases (2017)). For the SACs, although they demonstrate high ORR activities, the complex and time-consuming synthesis processes seriously limited their wide application. To achieve practical application at the MEA level, realizing industrial scale production is the main challenge that should be overcome.

5.2 Substrate optimization

Compared with ORR electrocatalysts, further investigations of the substrate are still insufficient at the current technology state. Reducing carbon corrosion and developing new materials are the two major research directions. The delight thing is that apart from carbon substrate, the tin oxide and titanium oxide have been

explored as the potential cathode and anode support materials, respectively, due to the high stability under high potentials. Under optimized conditions, the MEAs with TiO_2 and SnO_2-supported Pt catalysts can reach up to the equivalent performance of Pt/C. More importantly, they also demonstrated more stable activity under a higher potential (1.3 V) than C-supported catalysts [132].

5.3 Insight mechanism investigation

To explore the relationship between surface characteristics of catalysts and ORR dynamics, theoretical calculation is still the main method for most the reported works. Whereas, most of the models used in the DFT calculations are based on perfect crystal and without taking the real structure and reaction environment into account. Compared with DFT investigations, the evidence of insight into the catalytic mechanisms in experimentally is insufficient at the current technology state. Developing advanced characterization techniques, especially those *in situ operando* tools, is still the urgent issue. Generally, *in situ* characterization tools, such as X-ray photoelectron spectroscopy (XPS), low-energy electron diffraction (LEED), and scanning tunneling microscopy (STM), have been used in the reported papers. Very recently, Li et al. introduced a novel surface-enhanced Raman spectroscopic (SERS) "borrowing" strategy to explore the reaction intermediates for PtNi alloy catalysts during the ORR [133]. To investigate the changes of active sites of Fe-N-C, F. Jaouen et al. used ^{57}Fe Mössbauer spectroscopy to reveal the correlations between structure and activity of the catalyst [134]. These newly-developed techniques provided effective methods to investigate the *in situ* ORR catalytic process. Whereas, further efforts are still necessary. Based on the current research status, it is proposed that the DFT calculations should consider the real reaction conditions, which may provide more accurate information for the catalytic process or active sites. Combined with the experimental and theoretical results, further key information can be explored to the catalytic mechanisms and design robust catalysts.

5.4 Measurement conditions at MEA level

Considering the different measurement conditions between the RDE and MEA levels, it should be taking more effort to investigate the MEA-level or fuel cell activities of the ORR catalysts. Besides, the stability is another key point when evaluating an ORR catalyst, especially at a high reaction temperature rather than at room temperature, due to the MEA operating temperature is 60–80 °C. The durability targets set by DOE for stationary and transportation fuel cells are 40,000 and 5,000 h, respectively, under realistic operating conditions. In addition, it is necessary to develop a standard test protocol for the ORR catalyst at MEA level, such as the weight of used catalysts, reaction temperature, and gas flow, which can provide more accurate information when compared with different catalyst from different research groups.

5.5 Cost evaluation

Cost is the strongest market driver. Although numerous well-designed ORR catalysts have exceeded the performance of the benchmark of Pt/C, however, there is a long way to go to achieve practical application. Apart from the factor of stability, the cost is another crucial point that should be considered. The cost of catalysts has a directly relationship with the price of the raw materials and synthetic process. Therefore, apart from the price of precursor, the cost of synthesis process should also be carefully considered and calculated. However, in most of the reported works, the high cost of complex of synthesis process should usually be ignored. Therefore, up to now, it is a great challenge to calculate the price of the catalyst and select economical catalysts just based on the performance of reported ORR catalysts. Due to the complexity of calculating price, it can be proposed the factors such as precursors, synthesis conditions, and the product yields can be considered. In this way, an approximate cost of the synthesized catalysts can be obtained.

In conclusion, although ORR catalysts have achieved great progress, developing robust ORR catalysts applicated in PEMFCs urgently becomes a significant problem to meet the practical demand. Our work aims to put more emphasis on the discussion of designing robust catalysts at the MEA and full-cell level, aiming to help stimulate more attention on their practical application. We hope the discussion presented in this review can guide the design of more efficient catalysts for practical PEMFCs in near future.

Acknowledgements

We acknowledge the financial support by the Natural Science Foundation of Shandong Province (No. ZR202103040753) and the National Natural Science Foundation of China (No. 22102086).

References

[1] Lazaridis, T.; Stühmeier, B. M.; Gasteiger, H. A.; El-Sayed, H. A. Capabilities and limitations of rotating disk electrodes versus membrane electrode assemblies in the investigation of electrocatalysts. *Nat. Catal.* **2022**, *5*, 363–373.

[2] Sun, M. R.; Chen, C. L.; Wu, M. H.; Zhou, D. N.; Sun, Z. Y.; Fan, J. L.; Chen, W. X.; Li, Y. J. Rational design of Fe-N-C electrocatalysts for oxygen reduction reaction: From nanoparticles to single atoms. *Nano Res.* **2022**, *15*, 1753–1778.

[3] Guo, M. R.; Zhan, J.; Wang, Z. K.; Wang, X. R.; Dai, Z.; Wang, T. Supercapacitors as redox mediators for decoupled water splitting. *Chin. Chem. Lett.*, in press, https://doi.org/10.1016/j.cclet.2022.07.052.

[4] Liu, Z. Y.; Zhao, Z. P.; Peng, B. S.; Duan, X. F.; Huang, Y. Beyond extended surfaces: Understanding the oxygen reduction reaction on nanocatalysts. *J. Am. Chem. Soc.* **2020**, *142*, 17812–17827.

[5] Luo, E. G.; Chu, Y. Y.; Liu, J.; Shi, Z. P.; Zhu, S. Y.; Gong, L. Y.; Ge, J. J.; Choi, C. H.; Liu, C. P.; Xing, W. Pyrolyzed M-N_x catalysts for oxygen reduction reaction: Progress and prospects. *Energy Environ. Sci.* **2021**, *14*, 2158–2185.

[6] Kodama, K.; Nagai, T.; Kuwaki, A.; Jinnouchi, R.; Morimoto, Y. Challenges in applying highly active Pt-based nanostructured catalysts for oxygen reduction reactions to fuel cell vehicles. *Nat. Nanotechnol.* **2021**, *16*, 140–147.

[7] Zhou, M.; Wang, H. L.; Guo, S. J. Towards high-efficiency nanoelectrocatalysts for oxygen reduction through engineering advanced carbon nanomaterials. *Chem. Soc. Rev.* **2016**, *45*, 1273–1307.

[8] Zhao, C. X.; Liu, J. N.; Wang, J.; Ren, D.; Li, B. Q.; Zhang, Q. Recent advances of noble-metal-free bifunctional oxygen reduction and evolution electrocatalysts. *Chem. Soc. Rev.* **2021**, *50*, 7745–7778.

[9] Hou, C. C.; Wang, H. F.; Li, C. X.; Xu, Q. From metal-organic frameworks to single/dual-atom and cluster metal catalysts for energy applications. *Energy Environ. Sci.* **2020**, *13*, 1658–1693.

[10] Hou, C. C.; Xu, Q. Metal-organic frameworks for energy. *Adv. Energy Mater.* **2019**, *9*, 1801307.

[11] Tian, X. L.; Lu, X. F.; Xia, B. Y.; Lou, X. W. Advanced electrocatalysts for the oxygen reduction reaction in energy conversion technologies. *Joule* **2020**, *4*, 45–68.

[12] Kulkarni, A.; Siahrostami, S.; Patel, A.; Nørskov, J. K. Understanding catalytic activity trends in the oxygen reduction reaction. *Chem. Rev.* **2018**, *118*, 2302–2312.

[13] Calle-Vallejo, F.; Martínez, J. I.; García-Lastra, J. M.; Rossmeisl, J.; Koper, M. T. M. Physical and chemical nature of the scaling relations between adsorption energies of atoms on metal surfaces. *Phys. Rev. Lett.* **2012**, *108*, 116103.

[14] Bligaard, T.; Nørskov, J. K.; Dahl, S.; Matthiesen, J.; Christensen, C. H.; Sehested, J. The Brønsted–Evans–Polanyi relation and the volcano curve in heterogeneous catalysis. *J. Catal.* **2004**, *224*, 206–217.
[15] Nørskov, J. K.; Rossmeisl, J.; Logadottir, A.; Lindqvist, L.; Kitchin, J. R.; Bligaard, T.; Jónsson, H. Origin of the overpotential for oxygen reduction at a fuel-cell cathode. *J. Phys. Chem. B* **2004**, *108*, 17886–17892.
[16] Ross, P. N. Structure sensitivity in electrocatalytic properties of Pt: II. Oxygen reduction on low index single crystals and the role of steps. *J. Electrochem. Soc.* **1979**, *126*, 78–82.
[17] Marković, N. M.; Adžić, R. R.; Cahan, B. D.; Yeager, E. B. Structural effects in electrocatalysis: Oxygen reduction on platinum low index single-crystal surfaces in perchloric acid solutions. *J. Electroanal. Chem.* **1994**, *377*, 249–259.
[18] Attard, G. A.; Brew, A. Cyclic voltammetry and oxygen reduction activity of the Pt {110}-(1 × 1) surface. *J. Electroanal. Chem.* **2015**, *747*, 123–129.
[19] Kitchin, J. R.; Nørskov, J. K.; Barteau, M. A.; Chen, J. G. Modification of the surface electronic and chemical properties of Pt (111) by subsurface 3d transition metals. *J. Chem. Phys.* **2004**, *120*, 10240–10246.
[20] Stamenkovic, V.; Mun, B. S.; Mayrhofer, K. J. J.; Ross, P. N.; Markovic, N. M.; Rossmeisl, J.; Greeley, J.; Nørskov, J. K. Changing the activity of electrocatalysts for oxygen reduction by tuning the surface electronic structure. *Angew. Chem., Int. Ed.* **2006**, *45*, 2897–2901.
[21] Stamenkovic, V.; Schmidt, T. J.; Ross, P. N.; Markovic, N. M. Surface composition effects in electrocatalysis: Kinetics of oxygen reduction on well-defined Pt_3Ni and Pt_3Co alloy surfaces. *J. Phys. Chem. B* **2002**, *106*, 11970–11979.
[22] Stephens, I. E. L.; Bondarenko, A. S.; Perez-Alonso, F. J.; Calle-Vallejo, F.; Bech, L.; Johansson, T. P.; Jepsen, A. K.; Frydendal, R.; Knudsen, B. P.; Rossmeisl, J. et al. Tuning the activity of Pt (111) for oxygen electroreduction by subsurface alloying. *J. Am. Chem. Soc.* **2011**, *133*, 5485–5491.
[23] Luo, M. C.; Guo, S. J. Strain-controlled electrocatalysis on multimetallic nanomaterials. *Nat. Rev. Mater.* **2017**, *2*, 17059.
[24] Schlapka, A.; Lischka, M.; Groß, A.; Käsberger, U.; Jakob, P. Surface strain versus substrate interaction in heteroepitaxial metal layers: Pt on Ru (0001). *Phys. Rev. Lett.* **2003**, *91*, 016101.
[25] Strasser, P.; Koh, S.; Anniyev, T.; Greeley, J.; More, K.; Yu, C. F.; Liu, Z. C.; Kaya, S.; Nordlund, D.; Ogasawara, H. et al. Lattice-strain control of the activity in dealloyed core–shell fuel cell catalysts. *Nat. Chem.* **2010**, *2*, 454–460.
[26] Li, M. F.; Zhao, Z. P.; Cheng, T.; Fortunelli, A.; Chen, C. Y.; Yu, R.; Zhang, Q. H.; Gu, L.; Merinov, B. V.; Lin, Z. Y. et al. Ultrafine jagged platinum nanowires enable ultrahigh mass activity for the oxygen reduction reaction. *Science* **2016**, *354*, 1414–1419.
[27] Wang, X.; Vara, M.; Luo, M.; Huang, H. W.; Ruditskiy, A.; Park, J.; Bao, S. X.; Liu, J. Y.; Howe, J.; Chi, M. F. et al. Pd@Pt core–shell concave decahedra: A class of catalysts for the oxygen reduction reaction with enhanced activity and durability. *J. Am. Chem. Soc.* **2015**, *137*, 15036–15042.
[28] Zhang, L.; Roling, L. T.; Wang, X.; Vara, M.; Chi, M. F.; Liu, J. Y.; Choi, S. I.; Park, J.; Herron, J. A.; Xie, Z. X. et al. Platinum-based nanocages with subnanometer-thick walls and well-defined, controllable facets. *Science* **2015**, *349*, 412–416.
[29] Stamenkovic, V. R.; Fowler, B.; Mun, B. S.; Wang, G. F.; Ross, P. N.; Lucas, C. A.; Markovic, N. M. Improved oxygen reduction activity on Pt_3Ni (111) via increased surface site availability. *Science* **2007**, *315*, 493–497.
[30] Greeley, J.; Stephens, I. E. L.; Bondarenko, A. S.; Johansson, T. P.; Hansen, H. A.; Jaramillo, T. F.; Rossmeisl, J.; Chorkendorff, I.; Nørskov, J. K. Alloys of platinum and early transition metals as oxygen reduction electrocatalysts. *Nat. Chem.* **2009**, *1*, 552–556.
[31] Zhang, J.; Fang, J. Y. A general strategy for preparation of Pt 3d-transition metal (Co, Fe, Ni) nanocubes. *J. Am. Chem. Soc.* **2009**, *131*, 18543–18547.
[32] Kim, J.; Lee, Y.; Sun, S. H. Structurally ordered FePt nanoparticles and their enhanced catalysis for oxygen reduction reaction. *J. Am. Chem. Soc.* **2010**, *132*, 4996–4997.
[33] Xu, D.; Liu, Z. P.; Yang, H. Z.; Liu, Q. S.; Zhang, J.; Fang, J. Y.; Zou, S. Z.; Sun, K. Solution-based evolution and enhanced methanol oxidation activity of monodisperse platinum-copper nanocubes. *Angew. Chem., Int. Ed.* **2009**, *48*, 4217–4221.
[34] Chen, J. Y.; Wiley, B.; McLellan, J.; Xiong, Y. J.; Li, Z. Y.; Xia, Y. N. Optical properties of Pd-Ag and Pt-Ag nanoboxes synthesized via galvanic replacement reactions. *Nano Lett.* **2005**, *5*, 2058–2062.
[35] Peng, Z. M.; Yang, H. Synthesis and oxygen reduction electrocatalytic property of Pt-on-Pd bimetallic heteronanostructures. *J. Am. Chem. Soc.* **2009**, *131*, 7542–7543.
[36] Wang, L.; Nemoto, Y.; Yamauchi, Y. Direct synthesis of spatially-controlled Pt-on-Pd bimetallic nanodendrites with superior electrocatalytic activity. *J. Am. Chem. Soc.* **2011**, *133*, 9674–9677.
[37] Teng, X. W.; Feygenson, M.; Wang, Q.; He, J. Q.; Du, W. X.; Frenkel, A. I.; Han, W. Q.; Aronson, M. Electronic and magnetic properties of ultrathin Au/Pt nanowires. *Nano Lett.* **2009**, *9*, 3177–3184.
[38] Ataee-Esfahani, H.; Wang, L.; Nemoto, Y.; Yamauchi, Y. Synthesis of bimetallic Au@Pt nanoparticles with Au core and nanostructured Pt shell toward highly active electrocatalysts. *Chem. Mater.* **2010**, *22*, 6310–6318.
[39] Zhang, J.; Yang, H. Z.; Fang, J. Y.; Zou, S. Z. Synthesis and oxygen reduction activity of shape-controlled Pt_3Ni nanopolyhedra. *Nano Lett.* **2010**, *10*, 638–644.
[40] Wu, J. B.; Zhang, J. L.; Peng, Z. M.; Yang, S. C.; Wagner, F. T.; Yang, H. Truncated octahedral Pt_3Ni oxygen reduction reaction electrocatalysts. *J. Am. Chem. Soc.* **2010**, *132*, 4984–4985.
[41] Wu, Y. E.; Cai, S. F.; Wang, D. S.; He, W.; Li, Y. D. Syntheses of water-soluble octahedral, truncated octahedral, and cubic Pt-Ni nanocrystals and their structure–activity study in model hydrogenation reactions. *J. Am. Chem. Soc.* **2012**, *134*, 8975–8981.
[42] Kuttiyiel, K. A.; Sasaki, K.; Choi, Y.; Su, D.; Liu, P.; Adzic, R. R. Nitride stabilized PtNi core–shell nanocatalyst for high oxygen reduction activity. *Nano Lett.* **2012**, *12*, 6266–6271.
[43] Sasaki, K.; Naohara, H.; Choi, Y.; Cai, Y.; Chen, W. F.; Liu, P.; Adzic, R. R. Highly stable Pt monolayer on PdAu nanoparticle electrocatalysts for the oxygen reduction reaction. *Nat. Commun.* **2012**, *3*, 1115.
[44] Stamenkovic, V. R.; Mun, B. S.; Arenz, M.; Mayrhofer, K. J. J.; Lucas, C. A.; Wang, G. F.; Ross, P. N.; Markovic, N. M. Trends in electrocatalysis on extended and nanoscale Pt-bimetallic alloy surfaces. *Nat. Mater.* **2007**, *6*, 241–247.
[45] Chen, C.; Kang, Y. J.; Huo, Z. Y.; Zhu, Z. W.; Huang, W. Y.; Xin, H. L.; Snyder, J. D.; Li, D. G.; Herron, J. A.; Mavrikakis, M. et al. Highly crystalline multimetallic nanoframes with three-dimensional electrocatalytic surfaces. *Science* **2014**, *343*, 1339–1343.
[46] Xie, M. H.; Lyu, Z.; Chen, R. H.; Shen, M.; Cao, Z. M.; Xia, Y. N. Pt-Co@Pt octahedral nanocrystals: Enhancing their activity and durability toward oxygen reduction with an intermetallic core and an ultrathin shell. *J. Am. Chem. Soc.* **2021**, *143*, 8509–8518.
[47] Gao, R. J.; Wang, J.; Huang, Z. F.; Zhang, R. R.; Wang, W.; Pan, L.; Zhang, J. F.; Zhu, W. K.; Zhang, X. W.; Shi, C. X. et al. Pt/Fe_2O_3 with Pt–Fe pair sites as a catalyst for oxygen reduction with ultralow Pt loading. *Nat. Energy* **2021**, *6*, 614–623.
[48] Yoshida, T.; Kojima, K. Toyota MIRAI fuel cell vehicle and progress toward a future hydrogen society. *Electrochem. Soc. Interface* **2015**, *24*, 45–49.
[49] Liang, J. S.; Zhao, Z. L.; Li, N.; Wang, X. M.; Li, S. Z.; Liu, X.; Wang, T. Y.; Lu, G.; Wang, D. L.; Hwang, B. J. et al. Biaxial strains mediated oxygen reduction electrocatalysis on Fenton reaction resistant $L1_0$-PtZn fuel cell cathode. *Adv. Energy Mater.* **2020**, *10*, 2000179.
[50] Dai, Y.; Ou, L. H.; Liang, W.; Yang, F.; Liu, Y. W.; Chen, S. L. Efficient and superiorly durable Pt-lean electrocatalysts of Pt-W alloys for the oxygen reduction reaction. *J. Phys. Chem. C* **2011**, *115*, 2162–2168.
[51] Luo, M. C.; Zhao, Z. L.; Zhang, Y. L.; Sun, Y. J.; Xing, Y.; Lv, F.; Yang, Y.; Zhang, X.; Hwang, S.; Qin, Y. N. et al. PdMo bimetallene for oxygen reduction catalysis. *Nature* **2019**, *574*, 81–85.
[52] Thompson, S. T.; Wilson, A. R.; Zelenay, P.; Myers, D. J.; More,

K. L.; Neyerlin, K. C.; Papageorgopoulos, D. ElectroCat: DOE's approach to PGM-free catalyst and electrode R&D. *Solid State Ion.* **2018**, *319*, 68–76.

[53] Chen, Y. J.; Ji, S. F.; Chen, C.; Peng, Q.; Wang, D. S.; Li, Y. D. Single-atom catalysts: Synthetic strategies and electrochemical applications. *Joule* **2018**, *2*, 1242–1264.

[54] Jasinski, R. A new fuel cell cathode catalyst. *Nature* **1964**, *201*, 1212–1213.

[55] Yeager, E. Electrocatalysts for O_2 reduction. *Electrochim. Acta* **1984**, *29*, 1527–1537.

[56] Sun, T.; Tian, B. B.; Lu, J.; Su, C. L. Recent advances in Fe (or Co)/N/C electrocatalysts for the oxygen reduction reaction in polymer electrolyte membrane fuel cells. *J. Mater. Chem. A* **2017**, *5*, 18933–18950.

[57] Zhang, P.; Sun, F.; Xiang, Z. H.; Shen, Z. G.; Yun, J.; Cao, D. P. ZIF-derived *in situ* nitrogen-doped porous carbons as efficient metal-free electrocatalysts for oxygen reduction reaction. *Energy Environ. Sci.* **2014**, *7*, 442–450.

[58] Wu, Z. S.; Chen, L.; Liu, J. Z.; Parvez, K.; Liang, H. W.; Shu, J.; Sachdev, H.; Graf, R.; Feng, X. L.; Müllen, K. High-performance electrocatalysts for oxygen reduction derived from cobalt porphyrin-based conjugated mesoporous polymers. *Adv. Mater.* **2014**, *26*, 1450–1455.

[59] Lee, J. S.; Park, G. S.; Kim, S. T.; Liu, M. L.; Cho, J. A highly efficient electrocatalyst for the oxygen reduction reaction: N-doped ketjenblack incorporated into Fe/Fe_3C-functionalized melamine foam. *Angew. Chem., Int. Ed.* **2013**, *52*, 1026–1030.

[60] Ai, K. L.; Liu, Y. L.; Ruan, C. P.; Lu, L. H.; Lu, G. M. Sp^2 C-dominant N-doped carbon sub-micrometer spheres with a tunable size: A versatile platform for highly efficient oxygen-reduction catalysts. *Adv. Mater.* **2013**, *25*, 998–1003.

[61] Wu, G.; More, K. L.; Johnston, C. M.; Zelenay, P. High-performance electrocatalysts for oxygen reduction derived from polyaniline, iron, and cobalt. *Science* **2011**, *332*, 443–447.

[62] Wan, X.; Liu, X. F.; Li, Y. C.; Yu, R. H.; Zheng, L. R.; Yan, W. S.; Wang, H.; Xu, M.; Shui, J. L. Fe-N-C electrocatalyst with dense active sites and efficient mass transport for high performance proton exchange membrane fuel cells. *Nat. Catal.* **2019**, *2*, 259–268.

[63] Jiao, L.; Li, J. K.; Richard, L. L.; Sun, Q.; Stracensky, T.; Liu, E. S.; Sougrati, M. T.; Zhao, Z. P.; Yang, F.; Zhong, S. C. et al. Chemical vapour deposition of Fe-N-C oxygen reduction catalysts with full utilization of dense Fe-N_4 sites. *Nat. Mater.* **2021**, *20*, 1385–1391.

[64] Qu, X. M.; Han, Y.; Chen, Y. H.; Lin, J. X.; Li, G.; Yang, J.; Jiang, Y. X.; Sun, S. G. Stepwise pyrolysis treatment as an efficient strategy to enhance the stability performance of Fe-N_x/C electrocatalyst towards oxygen reduction reaction and proton exchange membrane fuel cell. *Appl. Catal. B: Environ.* **2021**, *295*, 120311.

[65] Liu, K. X.; Qiao, Z.; Hwang, S.; Liu, Z. Y.; Zhang, H. G.; Su, D.; Xu, H.; Wu, G.; Wang, G. F. Mn- and N-doped carbon as promising catalysts for oxygen reduction reaction: Theoretical prediction and experimental validation. *Appl. Catal. B: Environ.* **2019**, *243*, 195–203.

[66] Wang, X. X.; Prabhakaran, V.; He, Y. H.; Shao, Y. Y.; Wu, G. Iron-free cathode catalysts for proton-exchange-membrane fuel cells: Cobalt catalysts and the peroxide mitigation approach. *Adv. Mater.* **2019**, *31*, 1805126.

[67] Yin, Y.; Shi, L.; Li, W. L.; Li, X. N.; Wu, H.; Ao, Z. M.; Tian, W. J.; Liu, S. M.; Wang, S. B.; Sun, H. Q. Boosting Fenton-like reactions via single atom Fe catalysis. *Environ. Sci. Technol.* **2019**, *53*, 11391–11400.

[68] Zhao, C. X.; Li, B. Q.; Liu, J. N.; Zhang, Q. Intrinsic electrocatalytic activity regulation of M-N-C single-atom catalysts for the oxygen reduction reaction. *Angew. Chem., Int. Ed.* **2021**, *60*, 4448–4463.

[69] He, Y. H.; Hwang, S.; Cullen, D. A.; Uddin, M. A.; Langhorst, L.; Li, B. Y.; Karakalos, S.; Jeremy Kropf, A.; Wegener, E. C.; Sokolowski, J. et al. Highly active atomically dispersed CoN_4 fuel cell cathode catalysts derived from surfactant-assisted MOFs: Carbon-shell confinement strategy. *Energy Environ. Sci.* **2019**, *12*, 250–260.

[70] Xie, X. H.; He, C.; Li, B. Y.; He, Y. H.; Cullen, D. A.; Wegener, E. C.; Kropf, A. J.; Martinez, U.; Cheng, Y. W.; Engelhard, M. H. et al. Performance enhancement and degradation mechanism identification of a single-atom Co-N-C catalyst for proton exchange membrane fuel cells. *Nat. Catal.* **2020**, *3*, 1044–1054.

[71] Olson, T. S.; Pylypenko, S.; Fulghum, J. E.; Atanassov, P. Bifunctional oxygen reduction reaction mechanism on non-platinum catalysts derived from pyrolyzed porphyrins. *J. Electrochem. Soc.* **2010**, *157*, B54–B63.

[72] Liu, K. X.; Kattel, S.; Mao, V.; Wang. G. F. Electrochemical and computational study of oxygen reduction reaction on nonprecious transition metal/nitrogen doped carbon nanofibers in acid medium. *J. Phys. Chem. C* **2016**, *120*, 1586–1596.

[73] Wu, G.; Johnston, C. M.; Mack, N. H.; Artyushkova, K.; Ferrandon, M.; Nelson, M.; Lezama-Pacheco, J. S.; Conradson, S. D.; More, K. L.; Myers, D. J. et al. Synthesis-structure-performance correlation for polyaniline-Me-C non-precious metal cathode catalysts for oxygenreduction in fuelcells. *J. Mater. Chem.* **2011**, *21*, 11392–11405.

[74] Gupta, S.; Zhao, S.; Wang, X. X.; Hwang, S.; Karakalos, S.; Devaguptapu, S. V.; Mukherjee, S.; Su, D.; Xu, H.; Wu, G. Quaternary FeCoNiMn-based nanocarbon electrocatalysts for bifunctional oxygen reduction and evolution: Promotional role of Mn doping in stability carbon. *ACS Catal* **2017**, *7*, 8386–8393.

[75] Zhang, W.; Mao, K. K.; Zeng, X. C. B-doped MnN_4-G nanosheets as bifunctional electrocatalysts for both oxygen reduction and oxygen evolution reactions. *ACS Sustainable Chem. Eng.* **2019**, *7*, 18711–18717.

[76] Lin, Z. Y.; Huang, H.; Cheng, L.; Yang, Y.; Zhang, R. R.; Chen, Q. W. Atomically dispersed Mn within carbon frameworks as high-performance oxygen reduction electrocatalysts for zinc-air battery. *ACS Sustainable Chem. Eng.* **2020**, *8*, 427–434.

[77] Bai, L.; Duan, Z. Y.; Wen, X. D.; Si, R.; Guan, J. Q. Atomically dispersed manganese-based catalysts for efficient catalysis of oxygen reduction reaction. *Appl. Catal. B: Environ.* **2019**, *257*, 117930.

[78] Li, F.; Han, G. F.; Noh, H. J.; Kim, S. J.; Lu, Y. L.; Jeong, H. Y.; Fu, Z. P.; Baek, J. B. Boosting oxygen reduction catalysis with abundant copper single atom active sites. *Energy Environ. Sci.* **2018**, *11*, 2263–2269.

[79] Li, J.; Chen, S. G.; Yang, N.; Deng, M. M.; Ibraheem, S.; Deng, J. H.; Li, J.; Li, L.; Wei, Z. D. Ultrahigh-loading zinc single-atom catalyst for highly efficient oxygen reduction in both acidic and alkaline media. *Angew. Chem., Int. Ed.* **2019**, *58*, 7035–7039.

[80] Luo, E. G.; Zhang, H.; Wang, X.; Gao, L. Q.; Gong, L. Y.; Zhao, T.; Jin, Z.; Ge, J. J.; Jiang, Z.; Liu, C. P. et al. Single-atom Cr-N_4 sites designed for durable oxygen reduction catalysis in acid media. *Angew. Chem., Int. Ed.* **2019**, *58*, 12469–12475.

[81] Chen, Z. G.; Gong, W. B.; Liu, Z. B.; Cong, S.; Zheng, Z. H.; Wang, Z.; Zhang, W.; Ma, J. Y.; Yu, H. S.; Li, G. H. et al. Coordination-controlled single-atom tungsten as a non-3d-metal oxygen reduction reaction electrocatalyst with ultrahigh mass activity. *Nano Energy* **2019**, *60*, 394–403.

[82] Chen, M. J.; He, Y. H.; Spendelow, J. S.; Wu, G. Atomically dispersed metal catalysts for oxygen reduction. *ACS Energy Lett.* **2019**, *4*, 1619–1633.

[83] Yeager, E. Dioxygen electrocatalysis: Mechanisms in relation to catalyst structure. *J. Mol. Catal.* **1986**, *38*, 5–25.

[84] El-Deab, M. S.; Ohsaka, T. Electrocatalytic reduction of oxygen at Au nanoparticles-manganese oxide nanoparticle binary catalysts. *J. Electrochem. Soc.* **2006**, *153*, A1365.

[85] Yang, Z.; Zhou, X. M.; Nie, H. G.; Yao, Z.; Huang, S. M. Facile construction of manganese oxide doped carbon nanotube catalysts with high activity for oxygen reduction reaction and investigations into the origin of their activity enhancement. *ACS Appl. Mater. Interfaces* **2011**, *3*, 2601–2606.

[86] Liang, Y. Y.; Li, Y. G.; Wang, H. L.; Zhou, J. G.; Wang, J.; Regier,

T.; Dai, H. J. Co_3O_4 nanocrystals on graphene as a synergistic catalyst for oxygen reduction reaction. *Nat. Mater.* **2011**, *10*, 780–786.

[87] Liang, Y. Y.; Wang, H. L.; Diao, P.; Chang, W.; Hong, G. S.; Li, Y. G.; Gong, M.; Xie, L. M.; Zhou, J. G.; Wang, J. et al. Oxygen reduction electrocatalyst based on strongly coupled cobalt oxide nanocrystals and carbon nanotubes. *J. Am. Chem. Soc.* **2012**, *134*, 15849–15857.

[88] Lai, J. P.; Huang, B. L.; Tang, Y. H.; Lin, F.; Zhou, P.; Chen, X.; Sun, Y. J.; Lv, F.; Guo, S. J. Barrier-free interface electron transfer on PtFe-Fe_2C Janus-like nanoparticles boosts oxygen catalysis. *Chem* **2018**, *4*, 1153–1166.

[89] Guo, J. J.; Mao, Z.; Yan, X. L.; Su, R.; Guan, P. F.; Xu, B. S.; Zhang, X. F.; Qin, G. W.; Pennycook, S. J. Ultrasmall tungsten carbide catalysts stabilized in graphitic layers for high-performance oxygen reduction reaction. *Nano Energy* **2016**, *28*, 261–268.

[90] Xiao, M. L.; Zhu, J. B.; Feng, L. G.; Liu, C. P.; Xing, W. Meso/macroporous nitrogen-doped carbon architectures with iron carbide encapsulated in graphitic layers as an efficient and robust catalyst for the oxygen reduction reaction in both acidic and alkaline solutions. *Adv. Mater.* **2015**, *27*, 2521–2527.

[91] Tian, X. L.; Luo, J. M.; Nan, H. X.; Fu, Z. Y.; Zeng, J. H.; Liao, S. J. Binary transition metal nitrides with enhanced activity and durability for the oxygen reduction reaction. *J. Mater. Chem. A* **2015**, *3*, 16801–16809.

[92] Tian, X. L.; Wang, L. J.; Chi, B.; Xu, Y. Y.; Zaman, S.; Qi, K.; Liu, H. F.; Liao, S. J.; Xia, B. Y. Formation of a tubular assembly by ultrathin $Ti_{0.8}Co_{0.2}N$ nanosheets as efficient oxygen reduction electrocatalysts for hydrogen-/metal-air fuel cells. *ACS Catal.* **2018**, *8*, 8970–8975.

[93] Hou, C. C.; Zou, L. L.; Xu, Q. A hydrangea-like superstructure of open carbon cages with hierarchical porosity and highly active metal sites. *Adv. Mater.* **2019**, *31*, 1904689.

[94] Singh, K. P.; Bae, E. J.; Yu, J. S. Fe-P: A new class of electroactive catalyst for oxygen reduction reaction. *J. Am. Chem. Soc.* **2015**, *137*, 3165–3168.

[95] Liu, H. T.; Guan, J. Y.; Yang, S. X.; Yu, Y. H.; Shao, R.; Zhang, Z. P.; Dou, M. L.; Wang, F.; Xu, Q. Metal-organic-framework-derived Co_2P nanoparticle/multi-doped porous carbon as a trifunctional electrocatalyst. *Adv. Mater.* **2020**, *32*, 2003649.

[96] Hou, C. C.; Zou, L. L.; Wang, Y.; Xu, Q. MOF-mediated fabrication of a porous 3d superstructure of carbon nanosheets decorated with ultrafine cobalt phosphide nanoparticles for efficient electrocatalysis and zinc-air batteries.. *Angew. Chem., Int. Ed.* **2020**, *59*, 21360–21366.

[97] Wang, H. F.; Tang, C.; Wang, B.; Li, B. Q.; Zhang, Q. Bifunctional transition metal hydroxysulfides: Room-temperature sulfurization and their applications in Zn-air batteries. *Adv. Mater.* **2017**, *29*, 1702327.

[98] Dou, S.; Tao, L.; Huo, J.; Wang, S. Y.; Dai, L. M. Etched and doped Co_9S_8/graphene hybrid for oxygen electrocatalysis. *Energy Environ. Sci.* **2016**, *9*, 1320–1326.

[99] Fu, X. G.; Gao, R.; Jiang, G. P.; Li, M.; Li, S.; Luo, D.; Hu, Y. F.; Yuan, Q. X.; Huang, W. X.; Zhu, N. et al. Evolution of atomic-scale dispersion of FeN_x in hierarchically porous 3D air electrode to boost the interfacial electrocatalysis of oxygen reduction in PEMFC. *Nano Energy* **2021**, *83*, 105734.

[100] Xia, B. Y.; Yan, Y.; Li, N.; Wu, H. B.; Lou, X. W.; Wang, X. A metal-organic framework-derived bifunctional oxygen electrocatalyst. *Nat. Energy* **2016**, *1*, 15006.

[101] Yin, P. Q.; Yao, T.; Wu, Y. E.; Zheng, L. R.; Lin, Y.; Liu, W.; Ju, H. X.; Zhu, J. F.; Hong, X.; Deng, Z. X. et al. Single cobalt atoms with precise N-coordination as superior oxygen reduction reaction catalysts. *Angew. Chem., Int. Ed.* **2016**, *55*, 10800–10805.

[102] Hou, C. C.; Zou, L. L.; Sun, L. M.; Zhang, K. X.; Liu, Z.; Li, Y. W.; Li, C. X.; Zou, R. Q.; Yu, J. H.; Xu, Q. Single-atom iron catalysts on overhang-eave carbon cages for high-performance oxygen reduction reaction. *Angew. Chem., Int. Ed.* **2020**, *59*, 7384–7389.

[103] Xie, X. Y.; Shang, L.; Xiong, X. Y.; Shi, R.; Zhang, T. R. Fe single-atom catalysts on MOF-5 derived carbon for efficient oxygen reduction reaction in proton exchange membrane fuel cells. *Adv. Energy Mater.* **2022**, *12*, 2102688.

[104] Banham, D.; Ye, S. Y. Current status and future development of catalyst materials and catalyst layers for proton exchange membrane fuel cells: An industrial perspective. *ACS Energy Lett.* **2017**, *2*, 629–638.

[105] Tian, X. L.; Xu, Y. Y.; Zhang, W. Y.; Wu, T.; Xia, B. Y.; Wang, X. Unsupported platinum-based electrocatalysts for oxygen reduction reaction. *ACS Energy Lett.* **2017**, *2*, 2035–2043.

[106] Tian, X. L.; Zhao, X.; Su, Y. Q.; Wang, L. J.; Wang, H. M.; Dang, D.; Chi, B.; Liu, H. F.; Hensen, E. J. M.; Lou, X. W. et al. Engineering bunched Pt-Ni alloy nanocages for efficient oxygen reduction in practical fuel cells. *Science* **2019**, *366*, 850–856.

[107] Chong, L. N.; Wen, J. G.; Kubal, J.; Sen, F. G.; Zou, J. X.; Greeley, J.; Chan, M.; Barkholtz, H.; Ding, W. J.; Liu, D. J. Ultralow-loading platinum-cobalt fuel cell catalysts derived from imidazolate frameworks. *Science* **2018**, *362*, 1276–1281.

[108] Zhao, Z. P.; Liu, Z. Y.; Zhang, A.; Yan, X. X.; Xue, W.; Peng, B. S.; Xin, H. L.; Pan, X. Q.; Duan, X. F.; Huang, Y. Graphene-nanopocket-encaged PtCo nanocatalysts for highly durable fuel cell operation under demanding ultralow-Pt-loading conditions. *Nat. Nanotechnol.* **2022**, *17*, 968–975.

[109] Li, J. R.; Sharma, S.; Liu, X. M.; Pan, Y. T.; Spendelow, J. S.; Chi, M. F.; Jia, Y. K.; Zhang, P.; Cullen, D. A.; Xi, Z. et al. Hard-magnet $L1_0$-CoPt nanoparticles advance fuel cell catalysis. *Joule* **2019**, *3*, 124–135.

[110] Yang, C. L.; Wang, L. N.; Yin, P.; Liu, J. Y.; Chen, M. X.; Yan, Q. Q.; Wang, Z. S.; Xu, S. L.; Chu, S. Q.; Cui, C. H. et al. Sulfur-anchoring synthesis of platinum intermetallic nanoparticle catalysts for fuel cells. *Science* **2021**, *374*, 459–464.

[111] Cheng, Q. Q.; Yang, S.; Fu, C. H.; Zou, L. L.; Zou, Z. Q.; Jiang, Z.; Zhang, J. L.; Yang, H. High-loaded sub-6 nm Pt1Co1 intermetallic compounds with highly efficient performance expression in PEMFCs. *Energy Environ. Sci.* **2022**, *15*, 278–286.

[112] Liu, M. L.; Lu, B. A.; Yang, G. G.; Yuan, P. F.; Xia, H. C.; Wang, Y. J.; Guo, K.; Zhao, S. Y.; Liu, J.; Yu, Y. et al. Concave Pt-Zn nanocubes with high-index faceted Pt skin as highly efficient oxygen reduction catalyst. *Adv. Sci.* **2022**, *9*, 2200147.

[113] Chen, R.; Shu, T.; Zhao, F. L.; Li, Y. F.; Yang, X. T.; Li, J. W.; Zhang, D. L.; Gan, L. Y.; Yao, K. X.; Yuan, Q. $PtCu_3$ nanoalloy@porous PWO_x composites with oxygen container function as efficient ORR electrocatalysts advance the power density of room-temperature hydrogen-air fuel cells. *Nano Res.* **2022**, *15*, 9010–9018.

[114] Yang, X. T.; Yao, K. X.; Ye, J. Y.; Yuan, Q.; Zhao, F. L.; Li, Y. F.; Zhou, Z. Y. Interface-rich three-dimensional Au-doped PtBi intermetallics as highly effective anode catalysts for application in alkaline ethylene glycol fuel cells. *Adv. Funct. Mater.* **2021**, *31*, 2103671.

[115] Zhao, F. L.; Zheng, L. R.; Yuan, Q.; Yang, X. T.; Zhang, Q. H.; Xu, H.; Guo, Y. L.; Yang, S.; Zhou, Z. Y.; Gu, L. et al. Ultrathin PdAuBiTe nanosheets as high-performance oxygen reduction catalysts for a direct methanol fuel cell device. *Adv. Mater.* **2021**, *33*, 2103383.

[116] Li, X.; Yao, K. X.; Zhao, F. L.; Yang, X. T.; Li, J. W.; Li, Y. F.; Yuan, Q. Interface-rich Au-doped PdBi alloy nanochains as multifunctional oxygen reduction catalysts boost the power density and durability of a direct methanol fuel cell device. *Nano Res.* **2022**, *15*, 6036–6044.

[117] Wang, X. L.; Li, J. W.; Yang, X. T.; Zhao, F. L.; Li, Y. F.; Zhang, D. L.; Gan, L. Y.; Yao, K. X.; Yuan, Q. Low-coordinated surface sites make truncated Pd tetrahedrons as robust ORR electrocatalysts outperforming Pt for DMFC devices. *Nano Res.* **2022**, *15*, 7951–7958.

[118] Miao, Z. P.; Wang, X. M.; Zhao, Z. L.; Zuo, W. B.; Chen, S. Q.; Li, Z. Q.; He, Y. H.; Liang, J. S.; Ma, F.; Wang, H. L. et al. Improving the stability of non-noble-metal M-N-C catalysts for proton-exchange-membrane fuel cells through M–N bond length and coordination regulation. *Adv. Mater.* **2021**, *33*, 2006613.

[119] Wan, X.; Liu, Q. T.; Liu, J. Y.; Liu, S. Y.; Liu, X. F.; Zheng, L. R.; Shang, J. X.; Yu, R. H.; Shui, J. L. Iron atom-cluster interactions

increase activity and improve durability in Fe-N-C fuel cells. *Nat. Commun.* **2022**, *13*, 2963.

[120] Yang, Z. J.; Yang, H. Z.; Shang, L.; Zhang, T. R. Ordered PtFeIr intermetallic nanowires prepared through a silica-protection strategy for the oxygen reduction reaction. *Angew. Chem., Int. Ed.* **2022**, *61*, e202113278.

[121] Nie, Y.; Li, L.; Wei, Z. D. Recent advancements in Pt and Pt-free catalysts for oxygen reduction reaction. *Chem. Soc. Rev.* **2015**, *44*, 2168–2201.

[122] Eberle, U.; Müller, B.; von Helmolt, R. Fuel cell electric vehicles and hydrogen infrastructure: Status 2012. *Energy Environ. Sci.* **2012**, *5*, 8780–8798.

[123] Ferreira, P. J.; La O', G. J.; Shao-Horn, Y.; Morgan, D.; Makharia, R.; Kocha, S.; Gasteiger, H. A. Instability of Pt/C electrocatalysts in proton exchange membrane fuel cells: A mechanistic investigation. *J. Electrochem. Soc.* **2005**, *152*, A2256.

[124] Borup, R.; Meyers, J.; Pivovar, B.; Kim, Y. S.; Mukundan, R.; Garland, N.; Myers, D.; Wilson, M.; Garzon, F.; Wood, D. et al. Scientific aspects of polymer electrolyte fuel cell durability and degradation. *Chem. Rev.* **2007**, *107*, 3904–3951.

[125] Guo, D. H.; Shibuya, R.; Akiba, C.; Saji, S.; Kondo, T.; Nakamura, J. Active sites of nitrogen-doped carbon materials for oxygen reduction reaction clarified using model catalysts. *Science* **2016**, *351*, 361–365.

[126] Zitolo, A.; Goellner, V.; Armel, V.; Sougrati, M. T.; Mineva, T.; Stievano, L.; Fonda, E.; Jaouen, F. Identification of catalytic sites for oxygen reduction in iron- and nitrogen-doped graphene materials. *Nat. Mater.* **2015**, *14*, 937–942.

[127] Prabhakaran, V.; Arges, C. G.; Ramani, V. Investigation of polymer electrolyte membrane chemical degradation and degradation mitigation using *in situ* fluorescence spectroscopy. *Proc. Natl. Acad. Sci. USA* **2012**, *109*, 1029–1034.

[128] Shao, Y. Y.; Dodelet, J. P.; Wu, G.; Zelenay, P. PGM-free cathode catalysts for PEM fuel cells: A mini-review on stability challenges. *Adv. Mater.* **2019**, *31*, 1807615.

[129] Wang, J.; Huang, Z. Q.; Liu, W.; Chang, C. R.; Tang, H. L.; Li, Z. J.; Chen, W. X.; Jia, C. J.; Yao, T.; Wei, S. Q. et al. Design of N-coordinated dual-metal sites: A stable and active Pt-free catalyst for acidic oxygen reduction reaction. *J. Am. Chem. Soc.* **2017**, *139*, 17281–17284.

[130] Deng, Y. J.; Chi, B.; Li, J.; Wang, G. H.; Zheng, L.; Shi, X. D.; Cui, Z. M.; Du, L.; Liao, S. J.; Zang, K. T. et al. Atomic Fe-doped MOF-derived carbon polyhedrons with high active-center density and ultra-high performance toward PEM fuel cells. *Adv. Energy Mater.* **2019**, *9*, 1802856.

[131] Zhao, K. M.; Liu, S. Q.; Li, Y. Y.; Wei, X. L.; Ye, G. Y.; Zhu, W. W.; Su, Y. K.; Wang, J.; Liu, H. T.; He, Z. et al. Insight into the mechanism of axial ligands regulating the catalytic activity of Fe-N_4 sites for oxygen reduction reaction. *Adv. Energy Mater.* **2022**, *12*, 2103588.

[132] Arai, T.; Takashi, O.; Amemiya, K.; Takahashi, T. Study of oxide supports for PEFC catalyst. *SAE Int. J. Alt. Power.* **2017**, *6*, 145–150.

[133] Ze, H.; Chen, X.; Wang, X. T.; Wang, Y. H.; Chen, Q. Q.; Lin, J. S.; Zhang, Y. J.; Zhang, X. G.; Tian, Z. Q.; Li, J. F. Molecular insight of the critical role of Ni in Pt-based nanocatalysts for improving the oxygen reduction reaction probed using an *in situ* SERS borrowing strategy. *J. Am. Chem. Soc.* **2021**, *143*, 1318–1322.

[134] Li, J. K.; Sougrati, M. T.; Zitolo, A.; Ablett, J. M.; Oğuz, I. C.; Mineva, T.; Matanovic, I.; Atanassov, P.; Huang, Y.; Zenyuk, I. et al. Identification of durable and non-durable FeN_x sites in Fe-N-C materials for proton exchange membrane fuel cells. *Nat. Catal.* **2021**, *4*, 10–19.